PLANT SCIENCES

Alterations in hormonal signals spatially coordinate distinct responses to DNA double-strand breaks in *Arabidopsis* roots

Naoki Takahashi[1], Soichi Inagaki[1†], Kohei Nishimura[1], Hitoshi Sakakibara[2,3], Ioanna Antoniadi[4], Michal Karady[4‡], Karin Ljung[4], Masaaki Umeda[1]*

Plants have a high ability to cope with changing environments and grow continuously throughout life. However, the mechanisms by which plants strike a balance between stress response and organ growth remain elusive. Here, we found that DNA double-strand breaks enhance the accumulation of cytokinin hormones through the DNA damage signaling pathway in the *Arabidopsis* root tip. Our data showed that activation of cytokinin signaling suppresses the expression of some of the *PIN-FORMED* genes that encode efflux carriers of another hormone, auxin, thereby decreasing the auxin signals in the root tip and causing cell cycle arrest at G_2 phase and stem cell death. Elevated cytokinin signaling also promotes an early transition from cell division to endoreplication in the basal part of the root apex. We propose that plant hormones spatially coordinate differential DNA damage responses, thereby maintaining genome integrity and minimizing cell death to ensure continuous root growth.

INTRODUCTION

Plant roots play a crucial role in water and nutrient uptake, anchorage to soil, and sensing of the rhizosphere environment. Since these functions have a substantial impact on overall plant growth, root development is precisely controlled in response to changing underground conditions. Environmental stresses usually inhibit root growth; salinity, oxidation, or heat stress severely retards root growth. Previous studies demonstrated that roots that encounter high levels of boron or aluminum, and soil-borne pathogens, suffer from DNA damage and exhibit a delay or cessation of cell division, thereby suppressing root growth (*1*–*3*). This is an active response to DNA damage that is governed by the cell cycle checkpoint mechanism, in which cell cycle progression is arrested at a specific stage to ensure DNA repair or to provoke cell death in severe cases. As do other eukaryotes, plants have two protein kinases, ATAXIA TELANGIECTASIA MUTATED (ATM) and ATM AND RAD3-RELATED (ATR), that sense DNA damage and trigger cell cycle checkpoints (*4*, *5*). ATM is activated by DNA double-strand breaks (DSBs), whereas ATR primarily senses single-strand DNA and replication stress caused by DNA replication fork blocking. In animals and fungi, DNA damage signals are transmitted to Checkpoint-1 (CHK1) and CHK2 kinases, and ATM, ATR, CHK1, and CHK2 phosphorylate and activate the tumor suppressor protein p53 (*6*). However, orthologs of CHK and p53 are missing in plants; instead, the plant-specific NAM, ATAF and CUC (NAC)–type transcription factor, named SUPPRESSOR OF GAMMA RESPONSE 1 (SOG1), plays a central role in transmitting the signal from ATM and ATR (*7*). SOG1 is phosphorylated and activated by ATM and ATR (*8*, *9*) and binds to the sequence CTT[N]$_7$AAG to induce the expression of target genes involved in DNA repair and recombination, cell cycle control, and plant immunity (*10*).

In *Arabidopsis* roots, cells actively divide and proliferate in the meristematic zone in the tip region. After several rounds of cell division, cells stop dividing and start endoreplication, in which DNA replication is repeated without mitosis or cytokinesis. Endoreplicating cells begin to elongate and constitute the transition zone and, eventually, start more rapid cell elongation through actin reorganization in the elongation/differentiation zone (*11*). It was shown that DSBs arrest the cell cycle at G_2 in the meristematic zone (*12*) and promote an early onset of endoreplication (*13*), reducing the meristem size and inhibiting root growth. At the same time, selective cell death is induced in stem cells, which reside in the most apical part of the growing root and surround the quiescent center (QC) cells, in response to DSBs (*14*). These DNA damage responses are under the control of the ATM-SOG1 pathway, although how distinct DNA damage responses are coordinated to ensure continuous root growth remains elusive. We showed previously that two repressor-type R1R2R3-Myb transcription factors (Rep-MYBs), MYB3R3 and MYB3R5, participate in DNA damage–induced G_2 arrest by suppressing the expression of G_2-M–specific genes (*12*). We have recently demonstrated that protein accumulation of Rep-MYBs is regulated by the transcription factors ANAC044 and ANAC085 (*15*), while cyclin-dependent kinases (CDKs) also play a crucial role in Rep-MYB accumulation; namely, Rep-MYBs phosphorylated by CDKs are targeted for degradation, whereas low CDK activity caused by DNA damage stabilizes Rep-MYB proteins, leading to G_2 arrest (*12*). However, it remains unclear how CDK activities are inhibited by DNA stress in the root tip. Although DNA damage induces the expression of several CDK inhibitors and represses the gene encoding activator-type R1R2R3-Myb transcription factor, which induces G_2-M–specific genes, these transcriptional responses are known to be insufficient for G_2 arrest (*10*, *12*, *15*). Therefore, some unknown

[1]Graduate School of Science and Technology, Nara Institute of Science and Technology, Takayama 8916-5, Ikoma, Nara 630-0192, Japan. [2]Plant Productivity Systems Research Group, RIKEN Center for Sustainable Resource Science, Suehiro 1-7-22, Tsurumi, Yokohama 230-0045, Japan. [3]Graduate School of Bioagricultural Sciences, Nagoya University, Furo-cho, Chikusa-ku, Nagoya 464-8601, Japan. [4]Department of Forest Genetics and Plant Physiology, Umeå Plant Science Centre, Swedish University of Agricultural Sciences, 90183 Umeå, Sweden.
*Corresponding author. Email: mumeda@bs.naist.jp
†Present address: Department of Biological Sciences, Graduate School of Science, The University of Tokyo, Hongo, Bunkyo-ku, Tokyo 113-0033, Japan.
‡Present address: Laboratory of Growth Regulators, Institute of Experimental Botany of the Czech Academy of Sciences and Faculty of Science of Palacký University, Šlechtitelů 27, CZ-78371 Olomouc, Czech Republic.

mechanism(s) should function in down-regulation of CDK activities under DNA stress. Moreover, how stem cell death and the early onset of endoreplication are induced also remains unexplained.

Cytokinin plant hormones participate in various developmental and physiological processes such as seed germination, flowering, and senescence (*16*). The initial step of cytokinin biosynthesis is catalyzed by adenosine triphosphate/adenosine diphosphate (ATP/ADP) ISOPENTENYLTRANSFERASES (IPTs), which produce ribosylated and phosphorylated precursors of N^6-(Δ^2-isopentenyl) adenine (iP) (*17*). These products are converted to ribosylated and phosphorylated forms of *trans*-zeatin by the action of CYP735A, which hydroxylates the trans-end of the prenyl side chain (*18*). LONELY GUYs (LOGs) are essential enzymes for converting these precursors to biologically active cytokinins (*19*). Previous studies demonstrated that cytokinins are systemically transported in *Arabidopsis*: iP types are moved from shoots to the root meristem via the phloem (*20*), and *trans*-zeatin types are transported from roots to shoots via the xylem (*18*). CYP735A2 is predominantly expressed in developing vascular tissues of roots, thereby converting iP to *trans*-zeatin type and supplying *trans*-zeatin types to shoots (*18*). The ABC transporter ABCG14 contributes to *trans*-zeatin–type cytokinin transport by facilitating xylem loading in roots (*21*).

Cytokinins are known to inhibit primary root growth and lateral root formation by suppressing the expression of the auxin efflux carrier *PIN-FORMED* (*PIN*) (*22*, *23*). We previously reported that DSBs inhibit lateral root formation and that this inhibition is partially suppressed in cytokinin biosynthesis or signaling mutants, suggesting the possibility that DNA damage regulates lateral root development through influencing cytokinin signaling (*24*). However, it had remained elusive whether cytokinin biosynthesis or signaling is directly targeted by DNA damage signals and how other hormones are associated with DNA damage responses. Consequently, the exact role of hormonal signaling in controlling distinct DNA damage responses in roots is still totally unknown. In this study, we found that DSBs increase the endogenous cytokinin level in *Arabidopsis* roots, thereby suppressing the expression of *PIN1*, *PIN3*, and *PIN4* and decreasing the auxin level in the meristematic zone. We propose that reduced auxin signaling is a key to cause G_2 arrest and stem cell death, while enhanced cytokinin signaling promotes the early onset of endoreplication, representing the mechanisms underlying spatial regulation of DNA damage responses by two plant hormones.

RESULTS

DSBs activate cytokinin signaling in roots

To test whether cytokinin signaling is affected by DNA damage in *Arabidopsis* root tips, we first examined the promoter activity of the cytokinin-inducible type-A *ARABIDOPSIS* RESPONSE REGULATOR (ARR) gene *ARR5* (*25*). Five-day-old *pARR5:GUS* seedlings were transferred onto a medium containing 8 μM DSB-inducing reagent zeocin (*26*) and subjected to β-glucuronidase (GUS) staining after 24 hours. GUS activity was increased in the vasculature around the boundary between the meristematic zone and the transition zone, vascular initial cells and their daughters, and the root cap (Fig. 1A and fig. S1). We also observed roots carrying the cytokinin response marker *Two Component Signaling Sensor new* (*TCSn*):*GFP*, which reflects the transcriptional activity of type-B response regulators (*27*). The expression pattern of this marker was similar to that of *pARR5:GUS*, except that green fluorescent protein (GFP) fluorescence was also detected in the epidermis (Fig. 1B). Quantification of GFP fluorescence revealed that the expression level was elevated by zeocin treatment in four epidermal cells above and below the boundary between the meristematic zone and the transition zone (Fig. 1C). A higher level of GFP fluorescence was also observed in vascular cells encompassing a 100-μm region around the boundary (Fig. 1D). The elevated expression of *pARR5:GUS* and *TCSn:GFP* was similarly observed when seedlings were treated with bleomycin (0.6 μg/ml), another DSB inducer (fig. S2) (*26*). Our time-course experiment showed that the *TCSn:GFP* signal increased after 12 hours of zeocin treatment in both the epidermis and the vasculature, while propidium iodide (PI)–stained dead cells appeared in vascular initial cells and their daughters after 24 hours (fig. S3), suggesting that activation of cytokinin signaling is an early response to DSBs. To confirm that enhanced cytokinin signaling is not a consequence of disorganized tissue structure caused by DNA damage, we observed the expression patterns of several cell type–specific markers, *pAHP6:GFP* (protoxylem), *pAPL:GFPer* (phloem), *pCO2:H2B-YFP* (cortex), *pSCR:GFP-SCR* (endodermis and QC), and *pWOX5:NLS-YFP* (QC) (fig. S4). Zeocin treatment induced stem cell death after 24 hours, as mentioned above, but did not change the expression pattern of any marker, indicating that our experimental conditions did not cause severe defects in root tissue organization. Increased expression of *TCSn:GFP* was also observed after 1.5 mM aluminum treatment for 24 hours, which is also known to cause DSBs (*1*), while expression patterns of the cell type–specific markers were not altered (fig. S5).

In response to DSBs, ATM phosphorylates and activates the plant-specific transcription factor SOG1, which then induces hundreds of genes to trigger DNA damage responses (*7*). We found that zeocin treatment increased *pARR5:GUS* expression in wild type (WT), but not in the *atm-2* or *sog1-1* knockout mutant (fig. S1). This indicates that activation of cytokinin signaling in roots is a programmed response to DSBs that requires the ATM-SOG1 pathway.

DSBs elevate cytokinin level in the root tip

In *Arabidopsis*, iP and *trans*-zeatin are perceived by three receptors, *ARABIDOPSIS* HISTIDINE KINASE 2 (AHK2), AHK3, and AHK4/CRE1. The cytokinin signal activates the transcription factors, type-B ARRs, via the His-Asp phosphorelay pathway (*16*). Previous studies demonstrated that the type-B response regulators *ARR1* and *ARR2* are expressed around the transition zone and up-regulate cytokinin signaling to promote cell differentiation and restrict the meristem size (*28*, *29*). However, our quantitative real-time polymerase chain reaction (qRT-PCR) data showed that neither *ARR1* nor *ARR2* was induced by zeocin in roots (fig. S6A). The marker lines *pARR1:ARR1-GUS* and *pARR2:ARR2-GUS* displayed no change in expression levels after zeocin treatment (fig. S6B). These results indicate that DSBs do not up-regulate *ARR1* or *ARR2* in roots.

We therefore examined whether the endogenous cytokinin level increases in response to DNA damage. Cytokinin content was separately measured in cells constituting the transition zone or the meristematic zone. We performed fluorescence-activated cell sorting (FACS) on protoplasts prepared from *ROOT CLAVATA HOMOLOG 1* (*RCH1*) *promoter:GFP* or *RCH2 promoter:CFP* reporter lines. Since the *RCH1* and *RCH2* promoters are active in the meristematic zone and the transition zone, respectively, both in the presence and absence of zeocin (fig. S7) (*28*), GFP- or cyan fluorescent protein (CFP)–expressing protoplasts are expected to be derived from each

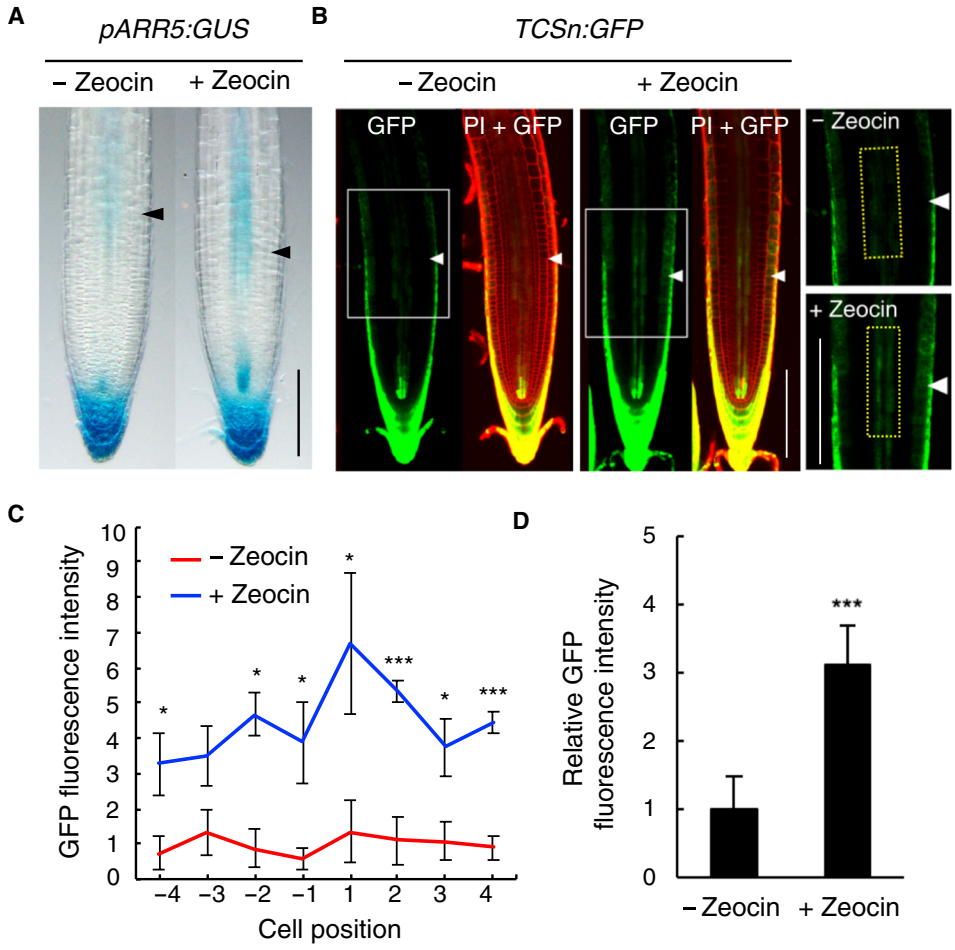

Fig. 1. DSBs activate cytokinin signaling in the root tip. (**A**) Zeocin response of the *ARR5* promoter activity. Five-day-old *pARR5:GUS* seedlings were transferred to Murashige and Skoog (MS) plates supplemented with (+ zeocin) or without (– zeocin) 8 μM zeocin and grown for 24 hours, followed by GUS staining. Arrowheads indicate the boundary between the meristematic zone and the transition zone. Scale bar, 100 μm. (**B**) Zeocin response of the synthetic cytokinin reporter *TCSn:GFP*. Five-day-old *TCSn:GFP* seedlings were treated with (+ zeocin) or without (– zeocin) 8 μM zeocin for 24 hours, and GFP fluorescence was observed after counterstaining with PI. Arrowheads indicate the boundary between the meristematic zone and the transition zone. Magnified images of the areas marked by white boxes are shown on the right [see also (D)]. Scale bars, 100 μm. (**C**) GFP fluorescence intensity in the root epidermis of *TCSn:GFP* seedlings. Cell position "1" indicates the first endoreplicated cell, which is preceded by the last mitotic cell before entry into the endoreplication (cell position "–1"). Data are presented as means ± SD ($n > 8$). Significant differences from the control without zeocin treatment were determined by Student's *t* test, $^{*}P < 0.05$ and $^{***}P < 0.001$. (**D**) GFP fluorescence intensity in the vasculature of *TCSn:GFP* seedlings. GFP fluorescence was measured in the areas surrounded by yellow dotted lines shown on the right in (B), which encompass a 100-μm region around the boundary between the meristematic zone and the transition zone. The value relative to that of the control without zeocin treatment is shown. Data are presented as means ± SD ($n = 10$). The significant difference from the control was determined by Student's *t* test, $^{***}P < 0.001$.

zone. Our cytokinin measurements revealed that, in the presence of zeocin, the levels of *trans*-zeatin, and cytokinin glucosides *trans*-zeatin-9-*N*-glucoside (*t*Z9G) and isopentenyladenosine-7-*N*-glucoside (iP7G), increased in the transition zone, but not in the meristematic zone (Fig. 2A). The amounts of cytokinin precursors *trans*-zeatin riboside and isopentenyladenosine riboside and cytokinin glucosides *trans*-zeatin-*O*-glucoside and *trans*-zeatin-7-*N*-glucoside (*t*Z7G) were elevated in both the meristematic zone and the transition zone, although the increases were higher in the transition zone (Fig. 2A). As a result, the total amount of *trans*-zeatin– and iP-type cytokinins was more markedly increased in the transition zone than the meristematic zone after zeocin treatment (Fig. 2B). We could not detect iP in any sample, probably because iP is efficiently degraded by CYTOKININ OXIDASE (CKX) enzymes and converted to *N*-glucosides (*30*).

DSB-dependent induction of cytokinin biosynthesis genes inhibits root growth

To identify the cause of the DNA damage–dependent increase in endogenous cytokinin content, we measured the transcript levels of 17 cytokinin biosynthesis genes: 7 ATP/ADP *IPT*s (*IPT1* and *IPT3*–*IPT8*), 2 *CYP735A*s (*CYP735A1* and *CYP735A2*), and 8 *LOG*s (*LOG1*–*LOG8*). We did not analyze tRNA *IPT*s (*IPT2* and *IPT9*) because they are engaged in the synthesis of *cis*-zeatin, a less physiologically active cytokinin than iP or *trans*-zeatin (*31*). qRT-PCR using RNA from whole seedlings revealed that zeocin treatment elevated the mRNA levels of *IPT1*, *IPT3*, *IPT5*, *IPT7*, *CYP735A2*, and *LOG7*, but not *LOG3*, *LOG4*, or *LOG8* (Fig. 3A). We could not detect transcripts of *IPT4*, *IPT6*, *IPT8*, *CYP735A1*, *LOG1*, *LOG2*, *LOG5*, or *LOG6* regardless of zeocin treatment. When qRT-PCR was conducted using RNA from roots, we could detect *LOG1* and

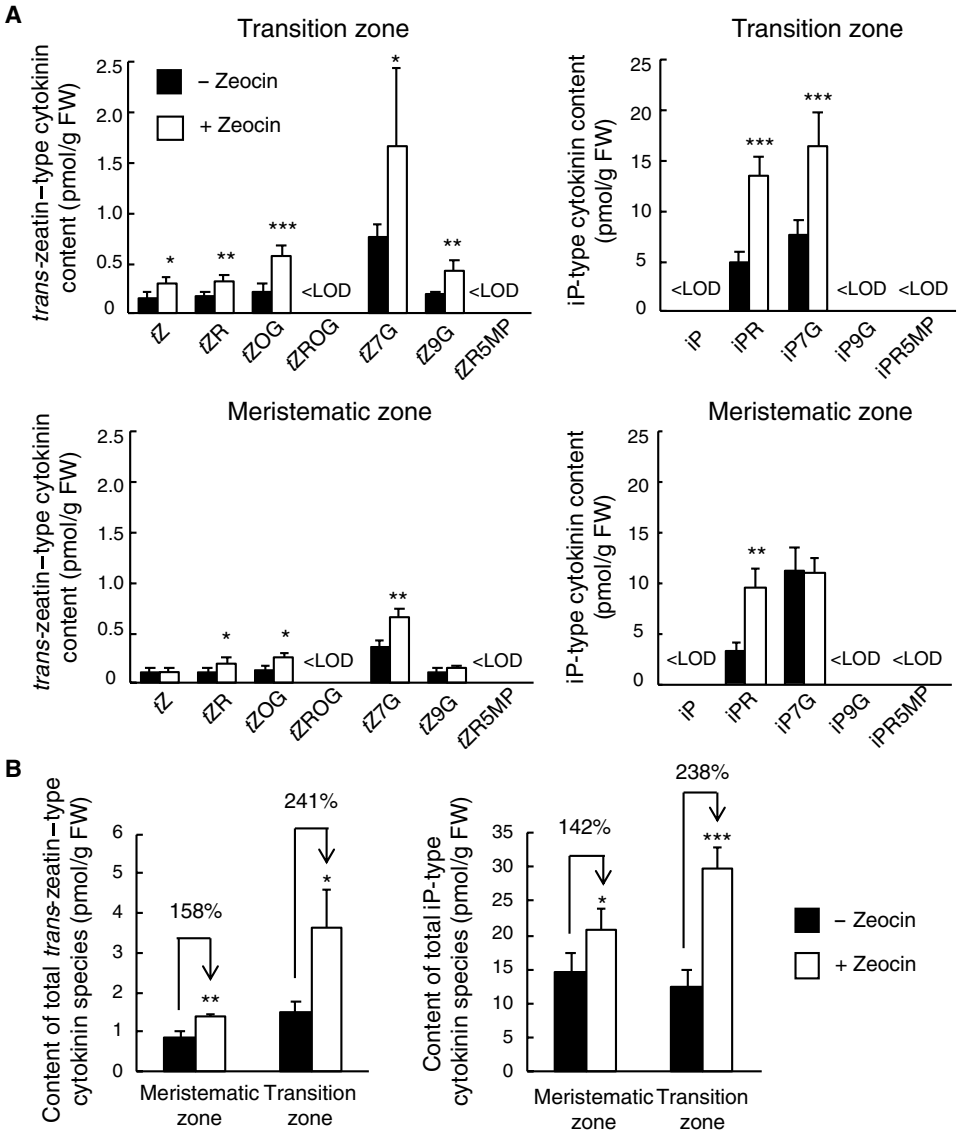

Fig. 2. DSBs elevate cytokinin level in the root tip. (**A** and **B**) Five-day-old seedlings of the marker lines *pRCH1:GFP* and *pRCH2:CFP* were transferred to MS plates with (+ zeocin) or without (– zeocin) 8 μM zeocin and grown for 24 hours. FACS was conducted to collect GFP- or CFP-positive protoplasts, which were analyzed for their cytokinin concentration using liquid chromatography–tandem mass spectrometry. Amounts of each *trans*-zeatin- and iP-type cytokinin per gram of fresh weight (FW) in GFP- or CFP-positive protoplasts, which were derived from cells in the meristematic zone or the transition zone, respectively (A), and those of total *trans*-zeatin– or iP-type cytokinin species (B) are shown. Data are presented as means ± SD ($n = 4$). Significant differences from the control without zeocin treatment were determined by Student's *t* test, $^{*}P < 0.05$, $^{**}P < 0.01$, and $^{***}P < 0.001$. <LOD, below limit of detection. *tZ*, *trans*-zeatin; *tZR*, *tZ* riboside; *tZOG*, *tZ-O*-glucoside; *tZROG*, *tZR-O*-glucoside; *tZ7G*, *tZ*-7-glucoside; *tZ9G*, *tZ*-9-glucoside; *tZR5MP*, *tZR*-5-monophosphate; iP, N^6-(Δ^2-isopentenyl) adenine; iPR, iP riboside; iP7G, iP-7-glucoside; iP9G, iP-9-glucoside; iPR5MP, iPR-5-monophosphate.

LOG5 transcripts; however, they were not increased by zeocin treatment (fig. S8A). Induction of *IPT1*, *IPT3*, *IPT5*, *IPT7*, *CYP735A2*, and *LOG7* was not observed in the *atm-2* or *sog1-1* mutant (fig. S8B), indicating that their induction is under the control of the ATM-SOG1 pathway. Although the *tZ*7G and *tZ*9G levels were elevated after zeocin treatment (Fig. 2A), the expression of the cytokinin *N*-glucosyltransferase *UGT76C2* that is involved in the formation of cytokinin glucosides was not induced at all (Fig. 3A), suggesting the possibility that DSBs enhance *trans*-zeatin production and consequently increase the *tZ*7G and *tZ*9G levels.

We then observed the expression patterns of the DSB-induced genes in tissues using the *promoter:GUS* reporter lines. *IPT1*, which is known to be expressed in the procambium (*32*), displayed increased expression in zeocin-treated root tips (Fig. 3C). The promoter activities of *IPT3* and *IPT5* were elevated in cotyledons and shoot apices, respectively, but not detected in the root tip (Fig. 3, B to D). *pIPT7:GUS* showed no GUS signal regardless of zeocin treatment, probably because the promoter region used for the reporter construction lacks essential cis-element(s). Zeocin highly induced *CYP735A2* and *LOG7* in the vasculature and in the epidermis and cortex, respectively, around the transition zone (Fig. 3, C and E). Consistent with the *TCSn:GFP* expression (fig. S3), the induction of *CYP735A2* and *LOG7* was observed after 12-hour zeocin treatment (fig. S9). These results suggest that zeocin taken up by roots induces

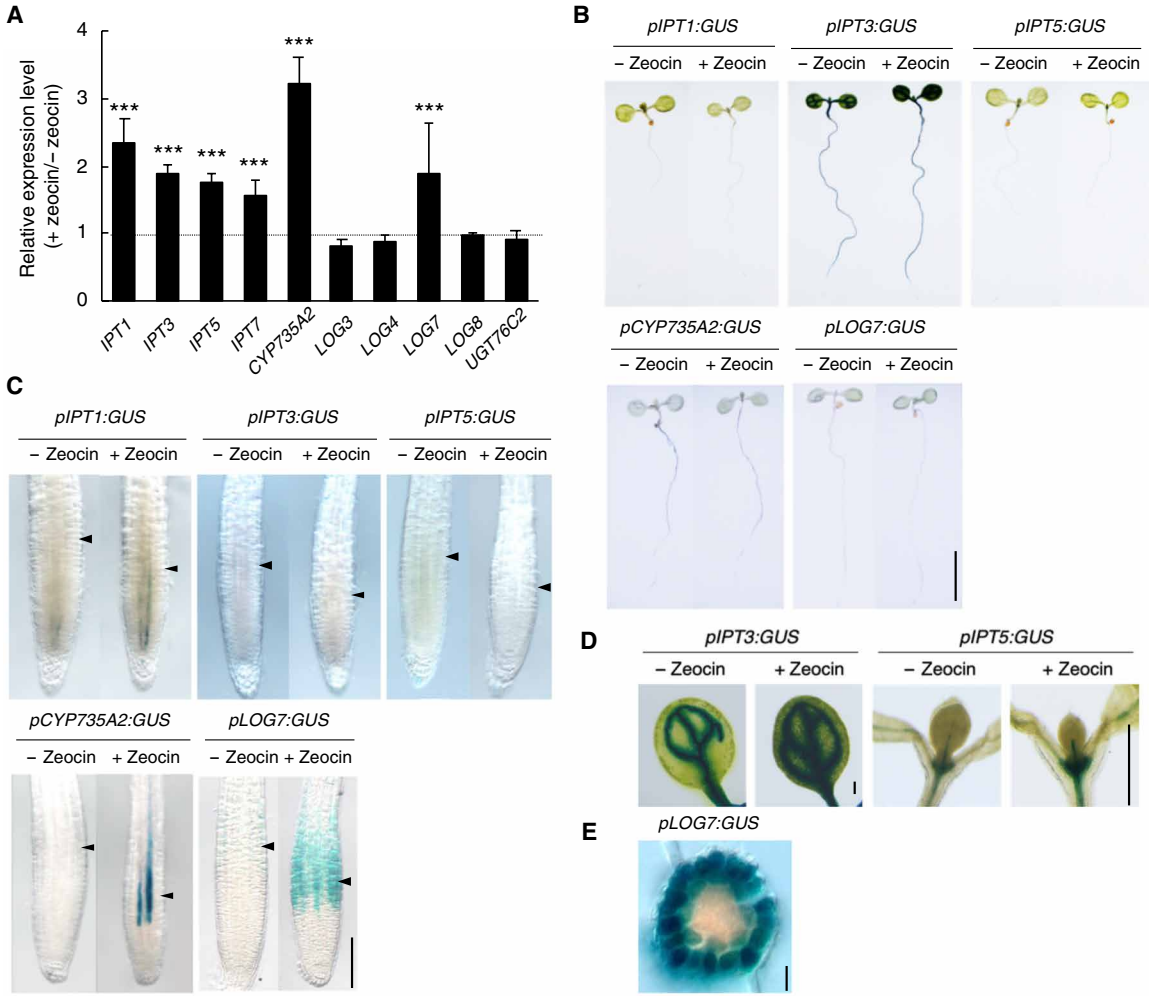

Fig. 3. DSBs induce cytokinin biosynthesis genes. (**A**) Transcript levels of cytokinin biosynthesis genes. Five-day-old WT seedlings were transferred to MS plates with or without 8 μM zeocin and grown for 24 hours. Total RNA was extracted from whole seedlings and subjected to qRT-PCR. Transcript levels of cytokinin biosynthesis genes were normalized to that of *ACTIN2* and are indicated as relative values, with that of the control without zeocin treatment set to 1. Data are presented as means ± SD calculated from three biological and technical replicates. Significant differences from the control were determined by Student's *t* test, ***$P < 0.001$. (**B** to **E**) Zeocin response of *pIPT1:GUS*, *pIPT3:GUS*, *pIPT5:GUS*, *pCYP735A2:GUS*, and *pLOG7:GUS*. Five-day-old seedlings were treated with (+ zeocin) or without (− zeocin) 8 μM zeocin for 24 hours. GUS-stained samples were observed for whole seedlings (B), root tips (C), and cotyledons and shoot apices (D). A cross section around the transition zone of zeocin-treated *pLOG7:GUS* is shown in (E). Arrowheads in (C) indicate the boundary between the meristematic zone and the transition zone. Scale bars, 1 cm (B), 100 μm (C), 1 mm (D), and 20 μm (E). Photo credits: Masaaki Umeda, Nara Institute of Science and Technology.

IPT3 and *IPT5* in shoots and provides more cytokinin precursors and that the induction of *CYP735A2* and *LOG7* around the transition zone leads to higher accumulation of iP- and *trans*-zeatin–type cytokinins in the root tip, as revealed by our cytokinin measurement (Fig. 2). The induction of *pLOG7:GUS* was also observed under DSB-causing aluminum stress (fig. S10).

We then examined whether the induction of cytokinin biosynthesis genes is involved in root growth inhibition in response to DNA damage. Since the *ipt1;3;5;7* quadruple mutant exhibits a severe growth defect (*17*), we used the *ipt3-2;5-1;7-1* triple mutant together with *cyp735a2-1* and *log7-1*. When 5-day-old seedlings were transferred onto a medium containing 8 μM zeocin, root growth was less severely inhibited in the three mutants than in WT (Fig. 4A). *ipt3-2;5-1;7-1* roots, which showed the highest zeocin tolerance, also grew faster than WT in the absence of zeocin (Fig. 4A), supporting the previous report that cytokinin precursors and active forms were markedly reduced in the triple mutant (*17*). Counting the cortical cell number in the meristematic zone showed that after zeocin treatment for 24 hours, the meristem size was reduced to 50% in WT, but only to 96, 78, and 79% in *ipt3-2;5-1;7-1*, *cyp735a2-1*, and *log7-1*, respectively (Fig. 4, B and C). We also measured the area of dead cells in the vasculature of PI-stained root tips. As shown in Fig. 4D, cell death area was markedly reduced in the three mutants as compared to WT. These results suggest that, although enhanced production of cytokinin precursors by IPT3 and IPT5 in shoots contributes to DSB-induced cytokinin accumulation in roots, CYP735A2- and LOG7-mediated synthesis of iP and *trans*-zeatin around the transition zone is crucial for root growth inhibition, reduction of the meristem size, and induction of stem cell death.

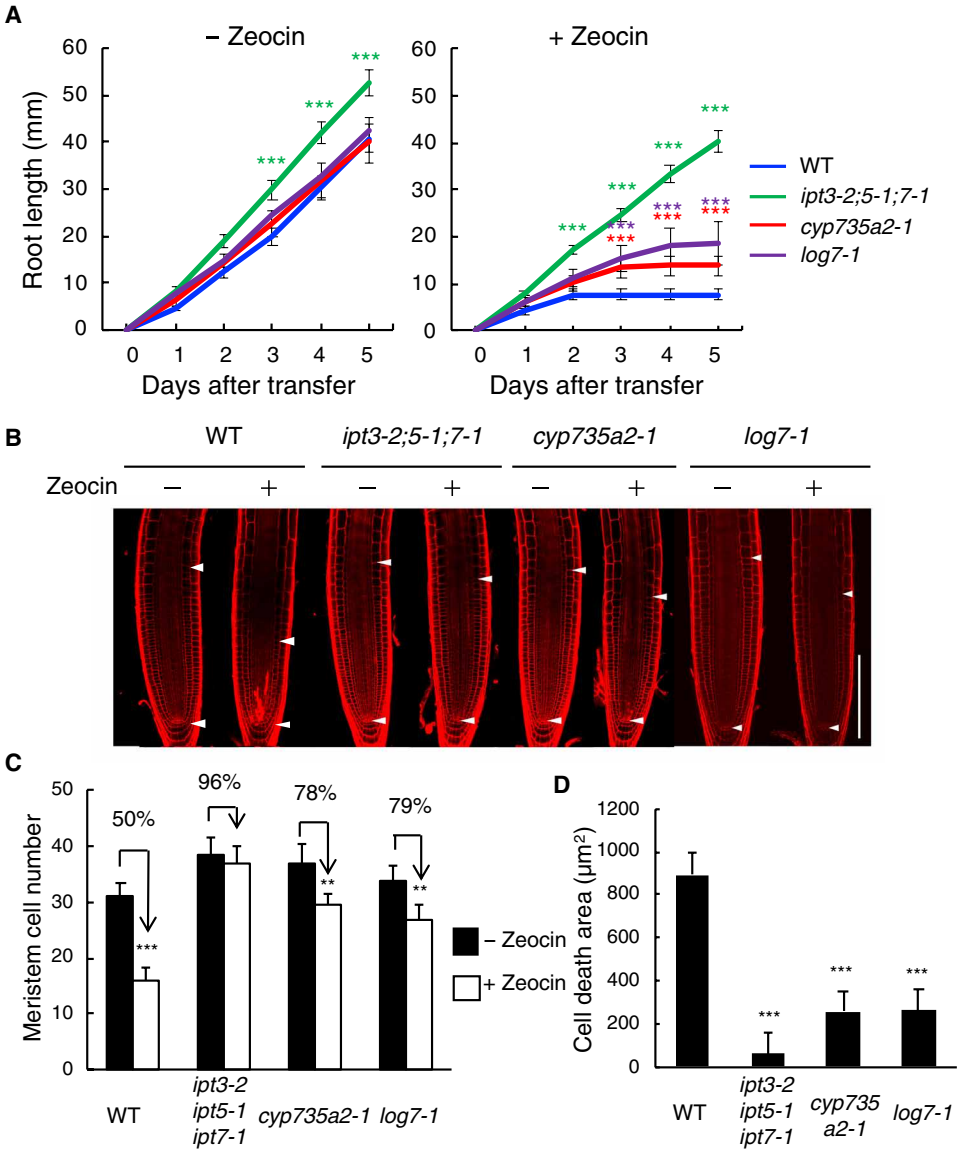

Fig. 4. Roots of cytokinin biosynthesis mutants are tolerant to DSBs. (**A**) Root growth of WT, *ipt3-2;5-1;7-1*, *cyp735a2-1*, and *log7-1*. Five-day-old seedlings were transferred to MS plates supplemented with (+ zeocin) or without (– zeocin) 8 μM zeocin, and root length was measured every 24 hours. Data are presented as means ± SD ($n > 20$). Significant differences from WT were determined by Student's *t* test, ***$P < 0.001$. (**B**) Images of root tips. Five-day-old seedlings were treated with (+) or without (–) 8 μM zeocin for 24 hours and subjected to PI staining. Arrowheads indicate the QC (bottom) and the boundary between the meristematic zone and the transition zone (top). Scale bar, 100 μm. (**C** and **D**) Cortical cell number in the meristematic zone and cell death area in vascular stem cells and their daughters. Five-day-old seedlings were treated with (+ zeocin) or without (– zeocin) 8 μM zeocin for 24 hours. The number of cortical cells between the QC and the first elongated cell was counted (C). The area of PI-stained dead cells in roots grown in the presence of zeocin was measured using ImageJ software (D). Data are presented as means ± SD ($n > 20$). Significant differences from the control without zeocin treatment (C) and WT (D) were determined by Student's *t* test, **$P < 0.01$ and ***$P < 0.001$.

Enhanced cytokinin signaling around the transition zone is involved in DSB-induced meristem size reduction and stem cell death

Cytokinin signaling is up-regulated around the transition zone of *Arabidopsis* roots due to localized expression of type-B ARRs (*28*). Therefore, we speculated that a reduction of the meristem size under DNA damage conditions is a consequence of enhanced cytokinin signaling around the transition zone, which is caused by higher cytokinin accumulation in the root tip. To test this possibility, we generated transgenic plants expressing *CKX1*, which encodes a cytokinin-degrading enzyme, in the transition zone under the *RCH2* promoter (fig. S11A). When 5-day-old seedlings were transferred onto zeocin-containing medium, root growth was only mildly inhibited in the two independent transgenic lines as compared with WT (fig. S11B). In the absence of zeocin, the cortical cell number in the meristematic zone was higher in *pRCH2:CKX1* than in WT (Student's *t* test, $P < 0.05$, $n > 20$) (fig. S11, C and D), matching a previous report (*28*). The transgenic lines displayed less reduction of the meristem size after zeocin treatment, and similar lower sensitivity was also observed in zeocin-induced cell death that rapidly

occurs in vascular stem cells and their daughters (fig. S11, C to E). These results suggest that the activation of cytokinin signaling around the transition zone is associated with meristem size reduction and stem cell death after DNA damage.

DSBs reduce auxin signaling in the root tip

Under normal growth conditions, one of the causes of meristem size restriction is the ARR1/12-mediated induction of *SHORT HYPOCOTYL 2* (*SHY2*)/*IAA3*, which encodes a member of the Aux/IAA protein family of auxin signaling repressors, around the transition zone (*23*). *SHY2* promoter activity was elevated around the transition zone in response to zeocin treatment (fig. S12A). Moreover, the *shy2-31* loss-of-function mutant, which has a larger meristem than WT (*23*), exhibited higher tolerance to DNA damage: The reduction of the meristem size and the cell death induction by zeocin were partially suppressed in *shy2-31* (Student's *t* test, $P < 0.05$, $n > 20$) (fig. S12, B to D).

DSB-induced cell death occurs around the stem cell niche except in the *SHY2* expression domain, suggesting the possibility that SHY2-dependent down-regulation of *PIN* expression inhibits auxin transport and causes stem cell death as well as meristem size reduction (*23*). To test this possibility, we then examined the response of *PIN* genes to DNA damage. In roots, PIN1 and PIN4 are required for downward auxin flow in the stele, and PIN2 functions in upward transport in the lateral root cap (LRC) and the epidermis (*33*). PIN3 and PIN7 regulate downward auxin flow in the stele and redirection in the columella for lateral transport to the LRC and the epidermis (*33*). Our qRT-PCR data showed that the transcript levels of *PIN1*, *PIN3*, and *PIN4*, but not *PIN2* or *PIN7*, were reduced by 8 μM zeocin treatment (Fig. 5A). This result was supported by the analysis of *pPIN:PIN-GFP* reporter lines; in the absence of zeocin, PIN1-GFP and PIN3/4-GFP accumulate in the apical and basal parts of the vasculature, respectively (*33*), whereas the GFP fluorescence was markedly decreased by zeocin treatment (Fig. 5B and fig. S13). It is noteworthy that the PIN1-GFP signal diminished in the meristematic zone, although *SHY2* is induced in the transition zone, but not in the meristematic zone (fig. S12A). Since *PIN1* expression is up-regulated by auxin in a time- and concentration-dependent manner (*34*), it is likely that SHY2-mediated *PIN3* and *PIN4* (and *PIN1*) repression around the transition zone disturbs downward auxin flow, thereby reducing the auxin level and suppressing *PIN1* expression in the meristematic zone. On the other hand, no change in expression patterns/levels of PIN2-GFP or PIN7-GFP was observed after zeocin treatment (Fig. 5B).

We next investigated the auxin response using the auxin-responsive marker *DR5rev:GFP* (*35*) and the GFP reporter driven by the *IAA2* promoter (*20*), which is one of the primary downstream targets of auxin signaling. As shown in Fig. 6A, the *DR5rev:GFP* signal in the QC and columella cells, and the *pIAA2:GFP* signal in the vasculature, QC, and columella cells, were reduced by 24-hour zeocin treatment, indicating that DSBs decrease auxin signaling in the meristematic zone, QC, and columella. We also used the *R2D2* reporter line, in which the mDII-tdTomato:DII-3xVenus ratio indicates relative auxin levels (*36*). Our observation revealed that zeocin treatment reduced the auxin level in the root tip (Fig. 6, B and C), corresponding with the decrease in auxin signaling.

To examine the involvement of auxin regulation in the DRR, we used naphthylphthalamic acid (NPA), which inhibits polar auxin transport (*37*). When WT roots were treated with 10 μM NPA, the meristem size was reduced to the same extent as with 8 μM zeocin treatment (Fig. 6D). However, cotreatment with zeocin and NPA did not generate an additive effect, suggesting that down-regulation of auxin level in the root tip is crucial for DSB-induced meristem size reduction. Since the cellular pattern in the root tip of the *pin1;3;4* mutant is severely disorganized (*38*), we could not estimate phenotypic defects in the DNA damage responses. However, in the triple mutant that exhibits lower *IAA2* expression than WT, zeocin did not further reduce the expression level, suggesting that suppression of *PIN1*, *PIN3*, and *PIN4* is involved in the decrease of auxin signaling in the root tip after zeocin treatment (Fig. 6E). Notably, zeocin-induced repression of *PIN1*, *PIN3*, *PIN4*, and *IAA2* was not observed in the *atm-2* or *sog1-1* mutant (fig. S14).

Activation of cytokinin biosynthesis is crucial for reducing auxin signaling in the meristem

We then asked whether reduced auxin signaling in the meristematic zone is caused by enhanced cytokinin biosynthesis. Our expression analyses showed that zeocin-triggered repression of *PIN1*, *PIN3*, *PIN4*, and *IAA2* was suppressed in *ipt3-2;5-1;7-1*, *cyp735a2-1*, and *log7-1* (Fig. 7A). Moreover, PIN1-GFP accumulation was not decreased in *log7-1* after zeocin treatment (Fig. 7B). As described above, *LOG7* is specifically induced around the transition zone by DSBs (Fig. 3C), suggesting that enhanced biosynthesis of active cytokinins around the transition zone plays a pivotal role in perturbing downward auxin flow and decreasing auxin signaling in the meristematic zone.

Reduced auxin signaling triggers both G_2 arrest and stem cell death

We previously reported that DSBs arrest the cell cycle preferentially at G_2 in dividing cells (*16*). To test whether enhanced cytokinin biosynthesis is involved in G_2 arrest in the meristematic zone, we conducted 5-ethynyl-2′-deoxyuridine (EdU) incorporation experiments to monitor cell cycle progression. EdU is incorporated into newly synthesized DNA during the S phase. After EdU-labeled cells pass through G_2, cells that enter mitosis display mitotic figures (*12*, *15*). Five-day-old WT and *log7-1* seedlings treated with or without 8 μM zeocin for 12 hours were incubated with EdU for 15 min, and the number of EdU-labeled cells with mitotic figures in the meristematic zone was counted after 4 and 6 hours. In WT, the percentage of these cells was significantly reduced in zeocin-treated roots, indicating retardation of G_2 progression (Fig. 7C). However, in *log7-1*, we could not find any difference between zeocin-treated and nontreated samples (Fig. 7C). These data suggest that activation of cytokinin biosynthesis is associated with DSB-induced G_2 arrest in the meristematic zone.

We next asked whether reduced auxin signaling is the cause of DSB-induced G_2 arrest. To address this issue, we treated WT roots with indole-3-acetic acid (IAA) at 5 nM, a very low concentration that did not change the meristem size at all (Fig. 8, A and B). When 5 nM IAA was applied together with 8 μM zeocin, *LOG7* induction was observed similarly to the sole zeocin treatment (fig. S15), suggesting that 5 nM IAA does not affect DSB-dependent activation of cytokinin biosynthesis. However, IAA treatment partially suppressed zeocin-induced meristem size reduction, and EdU incorporation experiments showed that G_2 arrest was also suppressed in the presence of both zeocin and IAA (Fig. 8, A to C). Zeocin-induced cell death was rarely observed in IAA-treated roots (Fig. 8, A and D), suggesting that a reduction in auxin signaling causes stem cell death and G_2 arrest under DNA damage conditions.

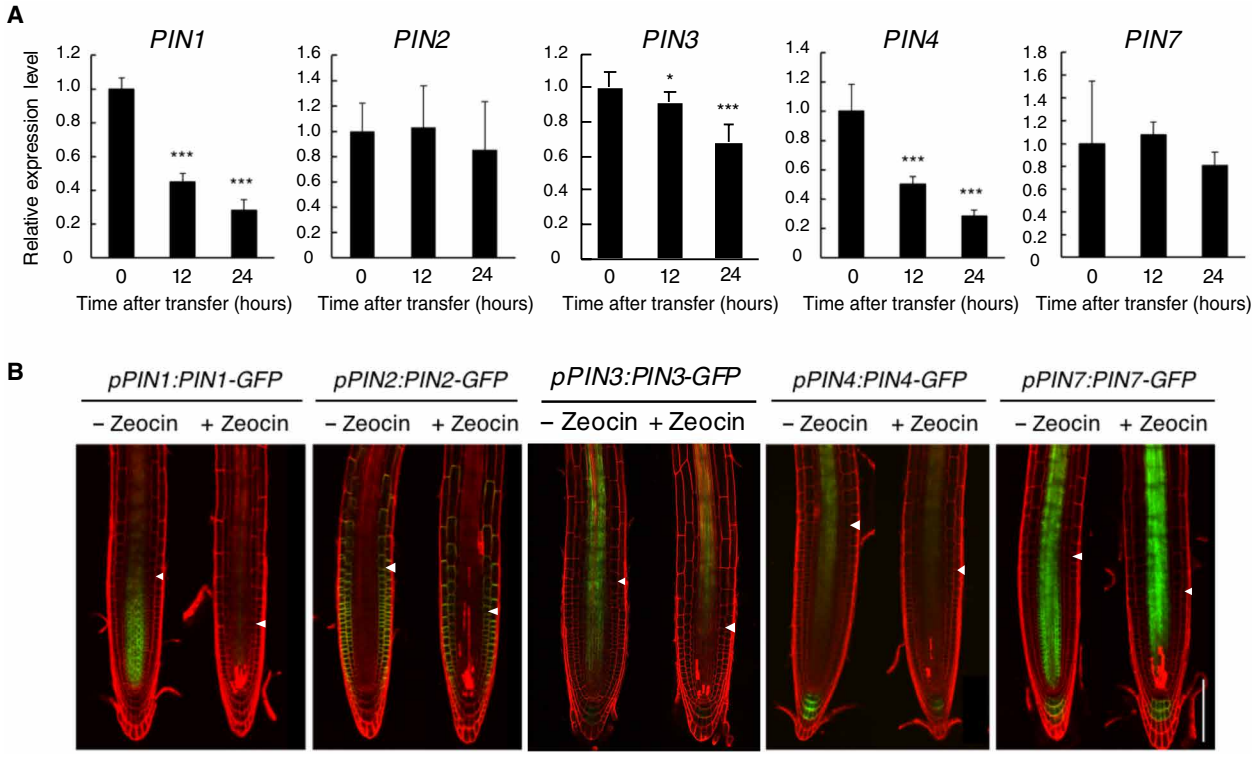

Fig. 5. DSBs inhibit expression of *PIN1*, *PIN3*, and *PIN4*. (**A**) Transcript levels of *PIN1*, *PIN2*, *PIN3*, *PIN4*, and *PIN7*. Five-day-old WT seedlings were transferred to MS plates containing 8 μM zeocin and grown for 0, 12, and 24 hours. Total RNA was extracted from roots and subjected to qRT-PCR. Transcript levels of *PIN1*, *PIN2*, *PIN3*, *PIN4*, and *PIN7* were normalized to that of *ACTIN2* and are indicated as relative values, with that for 0 hours set to 1. Data are presented as means ± SD calculated from three biological and technical replicates. Significant differences from the 0-hour sample were determined by Student's *t* test, $^{*}P < 0.05$ and $^{***}P < 0.001$. (**B**) Zeocin response of *pPIN1:PIN1-GFP*, *pPIN2:PIN2-GFP*, *pPIN3:PIN3-GFP*, *pPIN4:PIN4-GFP*, and *pPIN7:PIN7-GFP*. Five-day-old seedlings were treated with (+ zeocin) or without (– zeocin) 8 μM zeocin for 24 hours. GFP fluorescence was observed after counterstaining with PI. Arrowheads indicate the boundary between the meristematic zone and the transition zone. Scale bar, 100 μm.

A possible scenario is that the DSB-induced reduction of the auxin level triggers stem cell death, which consequently inhibits cell cycle progression in the meristematic zone. To examine this possibility, we activated auxin signaling in the vasculature under DNA stress. In the auxin receptor mutant *tir1-1*, we expressed *ccvTIR1*, which encodes a modified receptor that specifically recognizes the synthetic auxin cvxIAA and transmits the auxin signal (*39*) under the *WOODENLEG* promoter that is active in vascular stem cells and the stele (*40*). In the transgenic plants, auxin signaling is activated within the vascular tissue by cvxIAA treatment. Note that treatment with 10 nM cvxIAA alone affected neither the meristem size nor the G_2 progression in WT, *tir1-1*, or three independent transgenic lines (nos. 10, 25, and 34) (fig. S16, A and B). In the transgenic lines, 8 μM zeocin application reduced the meristem size and induced G_2 arrest irrespective of cvxIAA treatment, as observed in WT and *tir1-1* (fig. S16, A and B). This result is reasonable because we counted the meristem cell number and EdU-labeled cells with mitotic figures in the cortex and the epidermis, respectively, but not in the vasculature where *ccvTIR1* was expressed. However, zeocin-induced cell death was significantly suppressed by cvxIAA treatment in the transgenic lines (fig. S16C), indicating that up-regulation of auxin signaling in vascular stem cells suppresses zeocin-induced stem cell death, although this suppression cannot restore the defect in G_2 progression in the meristematic zone. In contrast, when *ccvTIR1* was expressed using the *TIR1* promoter, which is active throughout the root tip (*41*), cvxIAA treatment could suppress not only zeocin-induced cell death but also meristem size reduction and G_2 arrest (fig. S16, D to F). These results suggest that DSB-induced cell cycle arrest requires a reduction in auxin signaling but is not a consequence of stem cell death.

ARR2-CCS52A1 promotes an early onset of endoreplication in response to DNA damage

As mentioned above, the *shy2-31* mutation suppressed zeocin-induced meristem size reduction, but only partially (fig. S12, B and C). This suggests that in addition to SHY2-mediated inhibition of auxin signaling, another mechanism functions in meristem size control, probably through regulating the onset of endoreplication. We previously reported that cytokinin-activated ARR2, which is specifically expressed around the transition zone, induces the expression of *CELL CYCLE SWITCH PROTEIN 52 A1* (*CCS52A1*), encoding an activator of the E3 ubiquitin ligase anaphase-promoting complex/cyclosome (APC/C), and promotes degradation of mitotic cyclins, thereby enhancing the transition from cell division to endoreplication (*29*). Since cytokinins are elevated by DSBs as described above, it seemed likely that the ARR2-CCS52A1 pathway is associated with an early onset of endoreplication under DNA stress. To test this possibility, we first observed the promoter activity of *CCS52A1* using a GFP reporter line. As shown in Fig. 9A, the GFP signal in epidermal and cortical cells around the transition zone was significantly elevated

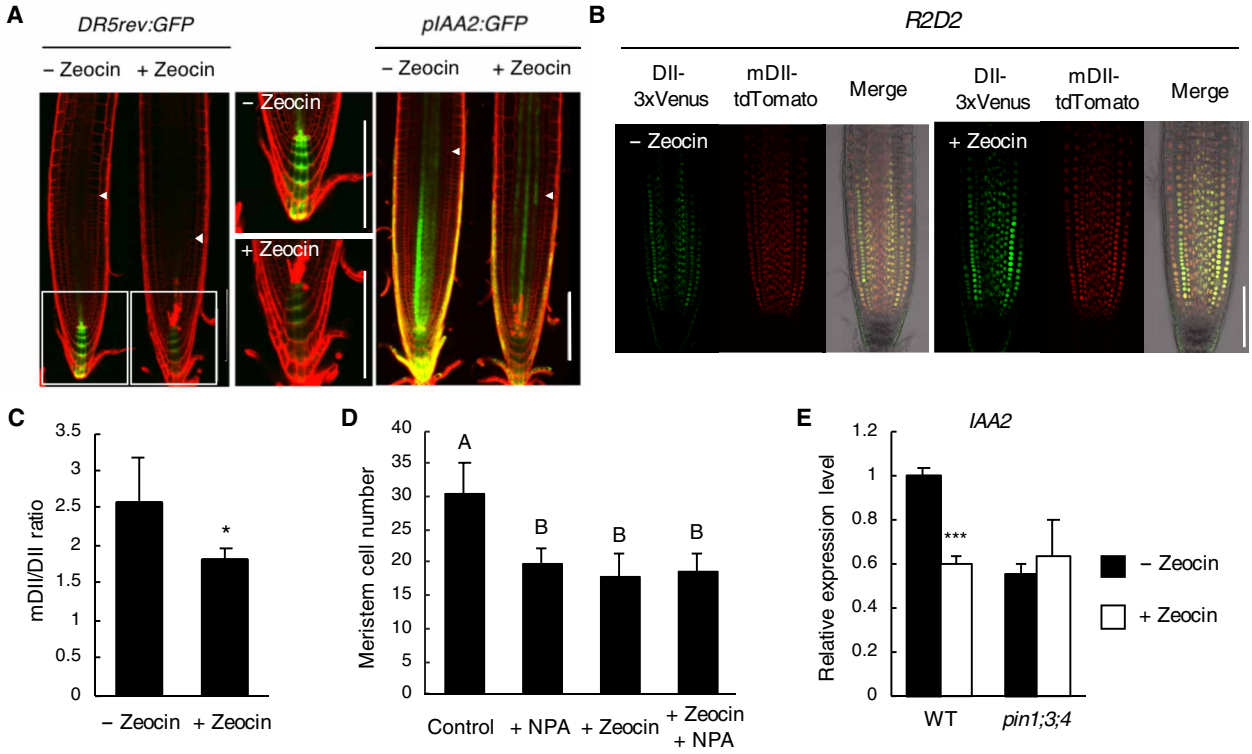

Fig. 6. DSBs inhibit auxin transport and signaling in the root tip. (**A**) Zeocin response of *DR5rev:GFP* and *pIAA2:GFP*. Five-day-old seedlings were treated with (+ zeocin) or without (– zeocin) 8 μM zeocin for 24 hours. Magnified images of the areas marked by white boxes in *DR5rev:GFP* are shown on the right. Arrowheads indicate the boundary between the meristematic zone and the transition zone. Scale bars, 100 μm. (**B** and **C**) Zeocin response of the *R2D2*. Five-day-old seedlings were treated with (+ zeocin) or without (– zeocin) 8 μM zeocin for 24 hours, and DII-3xVenus and mDII-tdTomato were observed (B). The fluorescence was measured in the meristematic zone, and the ratio of mDII-tdTomato:DII-3xVenus is shown (C). Data are presented as means ± SD ($n > 8$). The significant difference from the control without zeocin treatment was determined by Student's *t* test, $^*P < 0.05$. Scale bar, 100 μm. (**D**) Cortical cell number in the meristematic zone. Five-day-old seedlings were treated with or without 8 μM zeocin and/or 10 μM naphthylphthalamic acid (NPA) for 24 hours. The number of cortical cells between the QC and the first elongated cell was counted. Data are presented as means ± SD ($n > 18$). Bars with different alphabetical letters are significantly different from each other (Student's *t* test, $P < 0.05$). (**E**) *IAA2* transcript level in *pin1;3;4*. Five-day-old WT and *pin1;3;4* seedlings were transferred to MS plates with or without 8 μM zeocin and grown for 24 hours. Transcript levels of *IAA2* were normalized to that of *UBQ10* and are indicated as relative values, with that for the WT control without zeocin treatment set to 1. Data are presented as means ± SD calculated from three biological and technical replicates. Significant differences from the control without zeocin treatment were determined by Student's *t* test, $^{***}P < 0.001$.

after zeocin treatment. qRT-PCR revealed that *CCS52A1* transcripts increased by about fourfold in the presence of zeocin, while no such induction was observed in *atm-2*, *sog1-1*, *log7-1*, or *arr2-4* (Fig. 9, B and C), suggesting that *CCS52A1* is up-regulated through ARR2-mediated cytokinin signaling, which is activated by the higher accumulation of cytokinins. Zeocin-induced meristem size reduction was partially suppressed in the *ccs52a1-1* or *arr2-4* knockout mutant, and a similar level of suppression was observed for the *ccs52a1-1 arr2-4* double mutant (Fig. 9D), suggesting that the ARR2-CCS52A1 pathway enhances endoreplication onset and contributes to meristem size reduction.

To reveal whether the SHY2-dependent signaling and the ARR2/CCS52A1-mediated pathway cooperate in DSB-induced meristem size reduction, we performed genetic experiments. After zeocin treatment, the root meristem size was reduced to 44% in WT and to 63 and 55% in *arr2-4* and *shy2-31*, respectively, but only to 76% in the *arr2-4 shy2-31* double mutant (Fig. 9E). Similarly, the *ccs52a1-1 shy2-31* double mutant was less sensitive to zeocin than either single mutant (Fig. 9F). These results suggest that both ARR1/12-SHY2 and ARR2-CCS52A1 pathways function in meristem size control under DNA stress.

DISCUSSION

In this study, we revealed that DSB-stimulated ATM and SOG1 enhance cytokinin biosynthesis. As a result, cytokinin signaling is activated around the transition zone, and *SHY2* is up-regulated to repress *PIN1*, *PIN3*, and *PIN4*, thereby perturbing downward auxin flow. Reduction of auxin causes cell cycle arrest in the meristem and stem cell death. At the same time, ARR2 induces *CCS52A1* and promotes an early onset of endoreplication around the boundary between the meristematic zone and the transition zone. The combined effects of SHY2- and CCS52A1-dependent pathways reduce the root meristem size and, together with stem cell death, lead to root growth inhibition (Fig. 10). In plants, selective death of stem cells is a characteristic feature of the DNA damage response; in mammals, normal somatic cells undergo cell death in response to severe DNA damage (*42*). The genome integrity of stem cells needs to be highly maintained to ensure postembryonic organ development in plants. Therefore, stem cell death and the immediate supply of new stem cells from the organizing center, in which DNA repair genes are highly expressed (*43*), are a reasonable strategy to cope with DNA stress. On the other hand, cell death can disrupt the local tissue structure because plant cells do not migrate within tissues; thus,

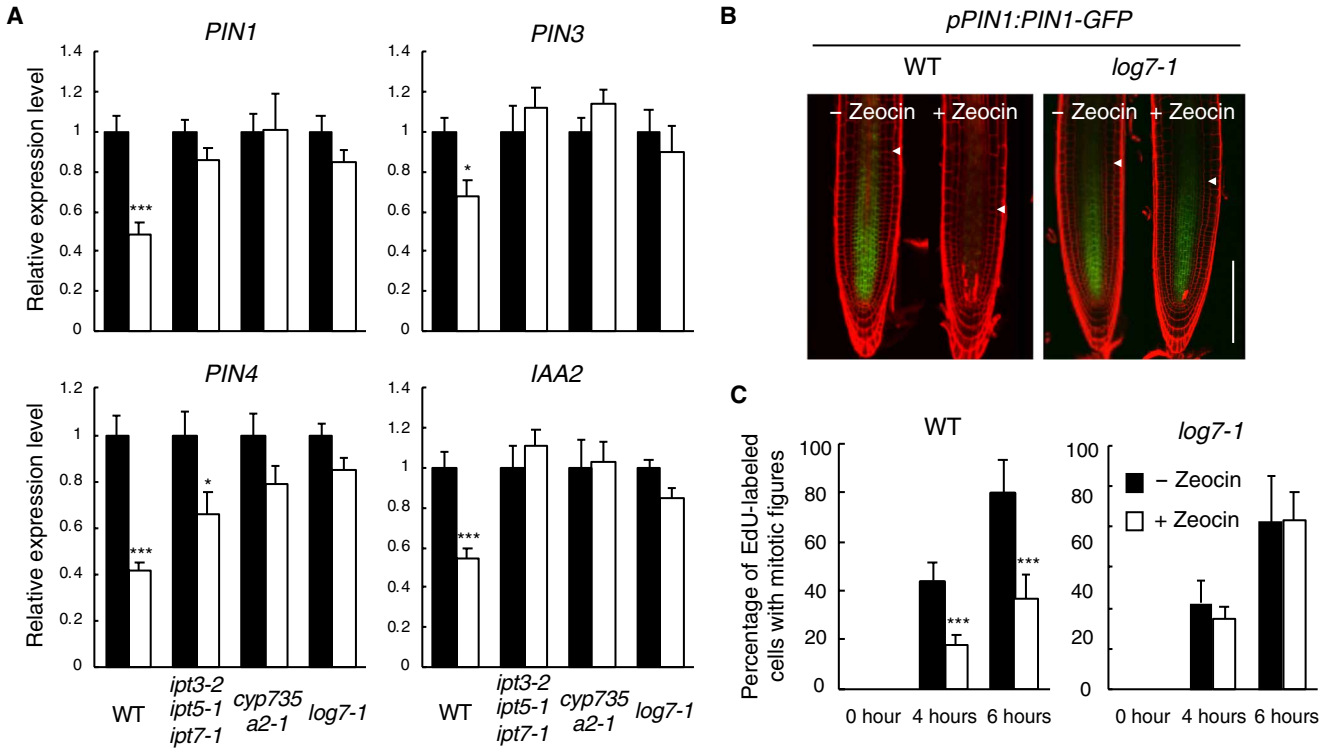

Fig. 7. LOG7 is involved in DSB-induced suppression of auxin flow and cell division. (**A**) Transcript levels of *PIN1*, *PIN3*, *PIN4*, and *IAA2* in *ipt3-2 ipt5-1 ipt7-1*, *cyp735a2-1*, and *log7-1*. Five-day-old seedlings were transferred to MS plates with or without 8 μM zeocin and grown for 24 hours. Total RNA was extracted from roots and subjected to qRT-PCR. Transcript levels of *PIN1*, *PIN3*, *PIN4*, and *IAA2* were normalized to that of *ACTIN2* and are indicated as relative values, with that for the control without zeocin treatment set to 1. Data are presented as means ± SD calculated from three biological and technical replicates. Significant differences from the control without zeocin treatment were determined by Student's *t* test, $^{*}P < 0.05$ and $^{***}P < 0.001$. (**B**) *PIN1-GFP* expression in *log7*. Five-day-old seedlings of WT and *log7-1* harboring *pPIN1:PIN1-GFP* were treated with (+ zeocin) or without (– zeocin) 8 μM zeocin for 24 hours. GFP fluorescence was observed after counterstaining with PI. Arrowheads indicate the boundary between the meristematic zone and the transition zone. Scale bar, 100 μm. (**C**) G_2 progression in *log7*. Five-day-old seedlings of WT and *log7-1* were transferred to MS plates with or without 8 μM zeocin and grown for 12 hours. After pulse labeling with 20 μM EdU for 15 min, seedlings were transferred back to MS plates with or without 8 μM zeocin and grown for 0, 4, and 6 hours. Cells in the meristematic zone were double-stained with ethynyl deoxyuridine (EdU) and 4′,6-diamidino-2-phenylindole (DAPI), and the percentage of EdU-labeled cells among those with mitotic figures was calculated. Data are presented as means ± SD ($n > 8$). Significant differences from the control without zeocin treatment were determined by Student's *t* test, $^{***}P < 0.001$.

plants may prevent normal somatic cells from undergoing cell death and, instead, activate the cell cycle checkpoint and accelerate the transition to endoreplication, thereby reducing the number of dividing cells, which are particularly sensitive to DNA damage. The present study clearly indicates that two plant hormones, cytokinin and auxin, orchestrate the differential DNA damage responses in roots, enabling the maintenance of genome integrity and continuous organ growth.

It has been reported recently that cytokinin-activated ARR1 regulates root meristem size through the control of auxin quantity in the LRC by induction of GH3.17 and PIN5, which inactivate IAA and pump auxin from the cytoplasm into the endoplasmic reticulum, respectively (*44*). In the present study, we have not investigated the involvement of GH3.17 or PIN5 in the DNA damage response, but it is possible that enhanced cytokinin biosynthesis affects the auxin level in the LRC and reduces the meristem size. We previously reported that DSBs inhibit lateral root formation (*24*), although how and to what extent hormonal signals are associated with this response have remained unknown. It is probable that cytokinin signaling activated by DNA damage inhibits auxin flow, in a manner similar to that shown in this study, and disturbs the proper organization of the LR meristem. Further studies will answer the question of whether the mechanisms identified here are responsible for controlling growth of the whole root system under genotoxic stress conditions.

One of the key findings in this study is that DNA damage induces the cytokinin biosynthesis genes *IPT1*, *IPT3*, *IPT5*, *IPT7*, *LOG7*, and *CYP735A2*. Their promoters do not have the consensus sequence for SOG1 binding (*10*); therefore, downstream transcription factor(s) may be involved in their induction. However, we cannot exclude the possibility that some of these cytokinin biosynthesis genes are directly regulated by SOG1, because SOG1 can still bind to sequences with a few nucleotide substitutions in the consensus motif (*10*). The *promoter:GUS* lines showed that *IPT1* expression increased in zeocin-treated roots, while *IPT3* and *IPT5* were induced in cotyledons and shoot apices, respectively (Fig. 3). Since the *ipt3-2;5-1;7-1* triple mutant exhibited a zeocin-tolerant phenotype in roots (Fig. 4), it is conceivable that cytokinin precursors produced by IPT3 and IPT5 are transported from shoots to roots and promote the DNA damage response in the root tip (Fig. 10). In support of this hypothesis, the levels of cytokinin precursors were significantly elevated in the root tip after zeocin treatment (Fig. 2).

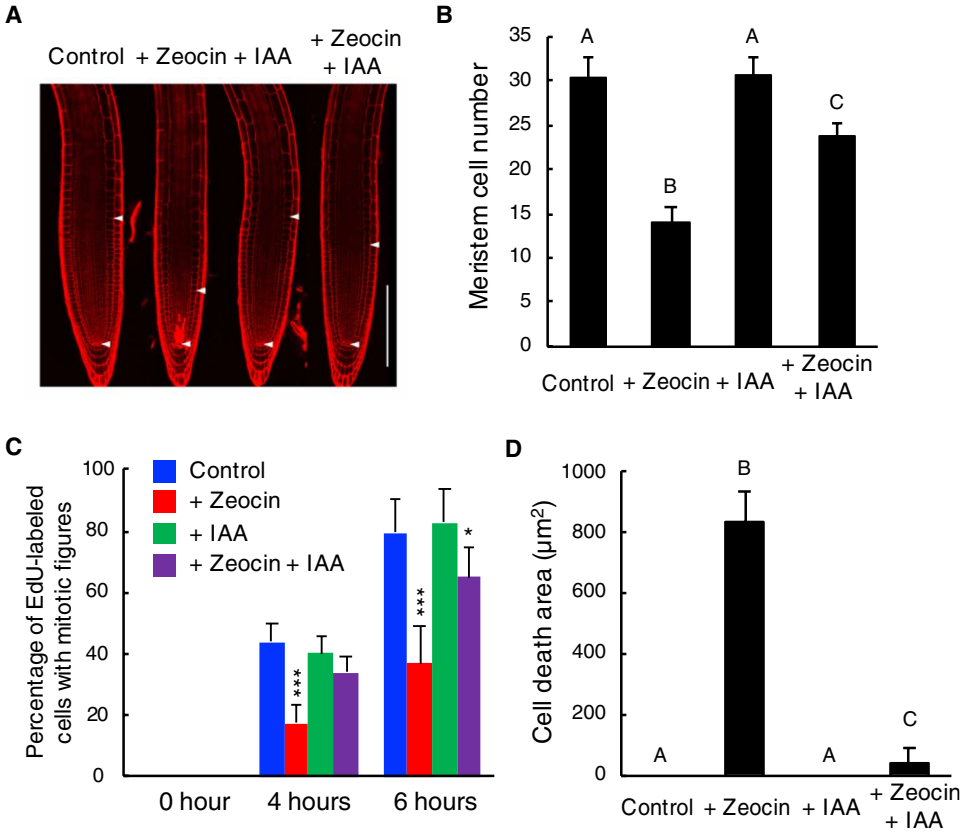

Fig. 8. DSB-induced reduction in auxin signaling causes G_2 arrest. (**A** and **B**) Root meristem size after treatment with zeocin and/or IAA. Five-day-old WT seedlings were transferred to MS plates supplemented with or without 8 μM zeocin and/or 5 nM IAA and grown for 24 hours. Arrowheads indicate the QC (bottom) and the boundary between the meristematic zone and the transition zone (top). Scale bar, 100 μm (A). The number of cortical cells between the QC and the first elongated cell was counted (B). Data are presented as means ± SD ($n > 20$). Bars with different alphabetical letters are significantly different from each other (Student's t test, $P < 0.01$). (**C**) G_2 progression in the presence of zeocin and/or IAA. Five-day-old WT seedlings were transferred to MS plates with or without 8 μM zeocin and/or 5 nM IAA and grown for 12 hours. After pulse labeling with 20 μM EdU for 15 min, seedlings were transferred back to MS plates with or without 8 μM zeocin and/or 5 nM IAA and grown for 0, 4, and 6 hours. Cells in the meristematic zone were double-stained with EdU and DAPI, and the percentage of EdU-labeled cells among those with mitotic figures was calculated. Data are presented as means ± SD ($n > 8$). Significant differences from the control without zeocin or IAA were determined by Student's t test, $^*P < 0.05$ and $^{***}P < 0.001$. (**D**) Cell death area in vascular stem cells and their daughters. Five-day-old WT seedlings were treated with or without 8 μM zeocin and/or 5 nM IAA for 24 hours, and the area of PI-stained dead cells was measured. Data are presented as means ± SD ($n > 20$). Bars with different alphabetical letters are significantly different from each other (Student's t test, $P < 0.01$).

However, it should be noted that zeocin in the solid medium is efficiently taken up by roots in our experimental system; therefore, how *IPT3/5* induction in shoots contributes to DNA damage responses in roots under natural environmental conditions remains obscure. DSBs also induce *CYP735A2* and *LOG7* specifically around the transition zone (Fig. 3), indicating that conversion from iP- to *trans*-zeatin–type cytokinins and the final activation step of cytokinin biosynthesis are enhanced around the transition zone. Note that LOG7 has the highest specificity constant (K_{cat}/K_m) among the eight LOG proteins in *Arabidopsis* (*19*), suggesting that *LOG7* induction facilitates efficient production of biologically active cytokinins around the transition zone, thereby enabling a rapid and strong response to DNA stress in terms of the control of meristem size and stem cell death. The *log7* mutant exhibited clear suppression in meristem size reduction; G_2 arrest; stem cell death; decreased expression of *PIN1*, *PIN3*, and *PIN4*; and induction of *CCS52A1* (Figs. 4, 7, and 9).

We previously reported that Rep-MYBs, which repress the expression of G_2-M–specific genes, play an essential role in inhibiting G_2 progression in response to DNA damage (*12*). Under normal growth conditions, CDKs phosphorylate Rep-MYBs and promote their degradation through the ubiquitin-proteasome pathway, leading to a release of transcriptional repression of G_2-M–specific genes. In response to DNA damage, CDK activity is reduced, and Rep-MYBs are stabilized to cause G_2 arrest (*12*). This model indicates that how CDK activity is suppressed is a key to trigger G_2 arrest when roots are exposed to DNA stress. The present study showed that DSBs activate cytokinin signaling around the transition zone and inhibit downward auxin flow, thereby decreasing the auxin level in the meristem, and that DSB-induced G_2 arrest occurred independently of stem cell death. Therefore, we propose that a decline in auxin level has a central role in reducing CDK activity and causing G_2 arrest. It has been shown that in *Arabidopsis*, auxin up-regulates the expression of *CDKA;1*, which encodes the functional ortholog of yeast Cdc2/Cdc28p (*45*). Genes for A2-type cyclins (CYCA2s), and for the CDK inhibitors KIP-RELATED PROTEIN 1 (KRP1) and KRP2, are induced and repressed, respectively, by exogenous auxin treatment (*46*), and the auxin antagonist α-(phenyl ethyl-2-one)-IAA

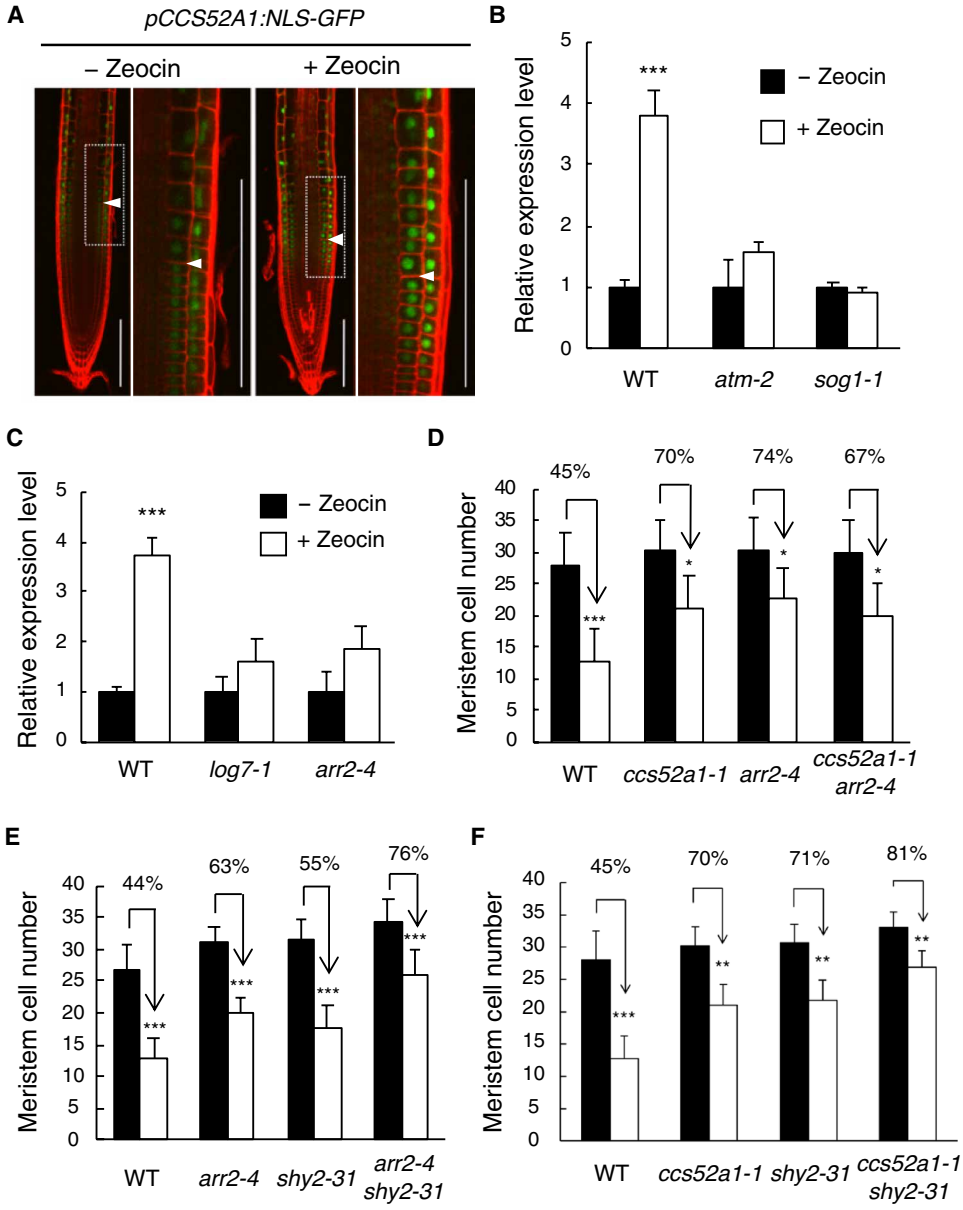

Fig. 9. The ARR2-CCS52A1 pathway participates in meristem size reduction caused by DSBs. (**A**) *CCS52A1* expression in the presence of zeocin. Five-day-old *pCCS52A1:NLS-GFP* seedlings were transferred to MS plates with (+ zeocin) or without (– zeocin) 8 μM zeocin and grown for 24 hours. GFP fluorescence was observed after counterstaining with PI. Arrowheads indicate the boundary between the meristematic zone and the transition zone. Magnified images of the areas marked by white boxes are shown on the right. Scale bars, 100 μm. (**B** and **C**) Transcript levels of *CCS52A1* in *atm*, *sog1*, *log7*, and *arr2*. Five-day-old seedlings were transferred to MS plates with or without 8 μM zeocin and grown for 24 hours. Total RNA was extracted from roots and subjected to qRT-PCR. Transcript levels of *CCS52A1* were normalized to that of *ACTIN2* and are indicated as relative values, with that for the control without zeocin treatment set to 1. Data are presented as means ± SD calculated from three biological and technical replicates. Significant differences from the control without zeocin treatment were determined by Student's *t* test, $^{***}P < 0.001$. (**D** to **F**) Cortical cell number in the meristematic zone. Five-day-old seedlings of WT, *ccs52a1-1*, *arr2-4*, *shy2-31*, *ccs52a1-1 arr2-4*, *arr2-4 shy2-31*, and *ccs52a1-1 shy2-31* were transferred to MS plates with or without 8 μM zeocin and grown for 24 hours. The number of cortical cells between the QC and the first elongated cell was counted. Data are presented as means ± SD ($n > 20$). Significant differences from the control without zeocin treatment were determined by Student's *t* test, $^{*}P < 0.05$, $^{**}P < 0.01$, and $^{***}P < 0.001$.

(PEO-IAA) rapidly decreased the transcript levels of *CDKB1;1* and *CYCA2;3* (*47*). Moreover, the heterodimeric transcription factor E2 PROMOTER BINDING FACTOR (E2F)-DIMERIZATION PARTNER (DP) is known to mediate auxin signaling and directly induce *CDKB1;1*, representing a clear connection between auxin and CDK expression (*48*, *49*). These observations suggest that a decline in auxin level leads to a reduction in overall CDK activities, thereby enabling stabilization of Rep-MYBs. Rep-MYBs are phosphorylated by all types of CDKs (A-, B1-, and B2-types) in *Arabidopsis* (*12*). Our recent study revealed that the transcription factors ANAC044 and ANAC085 are also involved in the control of Rep-MYB stability under DNA stress (*15*); therefore, the next important question is how

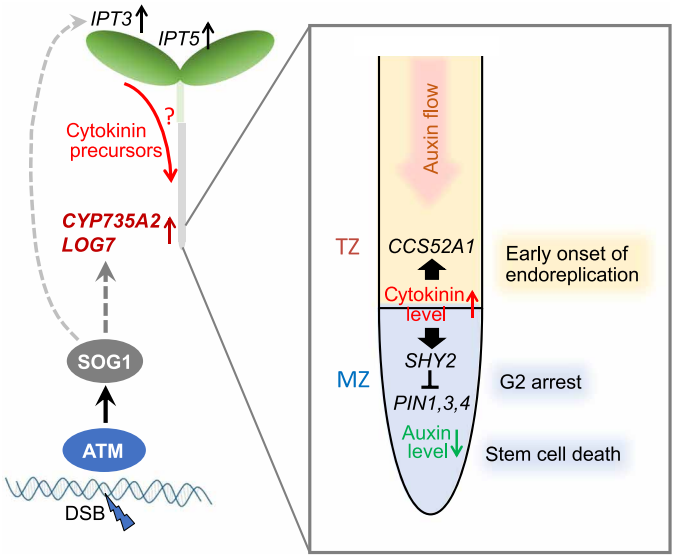

Fig. 10. Model for root meristem size reduction and stem cell death in response to DSBs. DSBs induce *IPT3* and *IPT5* in shoots and *CYP735A2* and *LOG7* in roots through the ATM-SOG1 pathway. Around the transition zone, conversion from iP- to *trans*-zeatin–type cytokinins and the final activation step of cytokinin biosynthesis are enhanced, resulting in an increase of active cytokinins. Elevated cytokinin signaling up-regulates *SHY2* and suppresses *PIN1*, *PIN3*, and *PIN4* expression, thereby inhibiting downward auxin flow and reducing the auxin level in the meristematic zone. This leads to G_2 arrest of dividing cells and stem cell death. Increased cytokinin signaling also up-regulates *CCS52A1* around the boundary between the meristematic zone and the transition zone and promotes degradation of mitotic cyclins, triggering an early onset of endoreplication. The combinatorial effect of G_2 arrest and an early transition from cell division to endoreplication causes meristem size reduction. TZ, transition zone; MZ, meristematic zone.

reduced auxin level and the ANAC044/085-dependent pathway cooperate in DNA damage–induced cell cycle arrest, which specifically occurs at G_2 phase.

Here, we revealed that a decrease in auxin signaling is one of the causes of stem cell death and cell cycle arrest under DNA stress. Canher *et al.* (*50*) recently reported that DSB-induced cell death obstructs auxin flow and facilitates auxin accumulation around dead cells, thereby enhancing stem cell regeneration. In this model, the regeneration process starts after cell death occurs, representing a scenario in which DSBs first reduce the auxin level in the meristematic zone and the stem cell niche, followed by a local auxin accumulation that contributes to stem cell regeneration. A key question regarding the initial event triggered by DNA damage is how reduced auxin signaling induces stem cell death. A previous study showed that treatment of cultured tobacco BY-2 cells with the auxin antagonist PEO-IAA resulted in chromatin relaxation (*51*) and that *Arabidopsis* mutants defective in the histone chaperone chromatin assembly factor-1 (CAF-1), which is involved in heterochromatin formation, accumulated high levels of DNA damage and frequently exhibited cell death in the root tip (*52*). Therefore, it is possible that reduced auxin signaling leads to chromatin decondensation, which makes the genome hypersensitive to DNA damage and promotes cell death. This is a fascinating hypothesis, but further research is essential to reveal how auxin controls the chromatin structure and the causal relationship between chromatin accessibility and DNA damage accumulation. Another interesting question is why only stem cells undergo cell death, although the auxin level decreases all over the meristematic zone. Lozano-Elena *et al.* (*53*) demonstrated that DSB-induced stem cell death was suppressed in the *Arabidopsis* mutant of *BRASSINOSTEROID INSENSITIVE 1* (*BRI1*), which encodes one of the brassinosteroid receptors, implying that another layer of regulation is necessary to give rise to stem cell–specific cell death. Further studies will deepen our understanding of how plants accomplish postembryonic organ development through maintaining genome stability under fluctuating environmental conditions.

MATERIALS AND METHODS

Plant growth conditions

Arabidopsis thaliana [ecotype Columbia-0 (Col-0)] plants were grown vertically under continuous light conditions at 22°C on Murashige and Skoog (MS) plates [0.5× MS salts, 2-(*N*-morpholino) ethanesulfonic acid (0.5 g/liter), 1% sucrose, and 1.2% phytoagar (pH 6.3)]. For DNA damage treatments, 5-day-old seedlings were transferred to new MS plates supplemented with or without 8 μM zeocin (Invitrogen Life Technologies) or bleomycin (0.6 μg/ml). For aluminum treatments, 5-day-old seedlings were transferred to new MS plus 5 mM succinic acid plates (pH 4.2) supplemented with or without 1.5 mM aluminum.

Plant materials and constructs

pARR5:GUS (*25*), *TCSn:GFP* (*27*), *atm-2* (*4*), *sog1-1* (*7*), *pAHP6:GFP* (*54*), *pAPL:GFPer* (*55*), *pCO2:H2B-YFP* (*56*), *pWOX5:NLS-YFP* (*57*), *pSCR:GFP-SCR* (*56*), *pRCH1:GFP* (*28*), *pRCH2:CFP* (*28*), *pARR1:ARR1-GUS* (*11*), *pARR2:ARR2-GUS* (*11*), *pIPT1:GUS* (*32*), *pIPT3:GUS* (*32*), *pIPT5:GUS* (*32*), *pCYP735A2:GUS* (*18*), *pLOG7:GUS* (*19*), *ipt3-2;5-1;7-1* (*17*), *cyp735a2-1* (*18*), *log7-1* (*19*), *pSHY2:GUS* (*58*), *pPIN1:PIN1-GFP* (*33*), *pPIN2:PIN2-GFP* (*33*), *pPIN3:PIN3-GFP* (*33*), *pPIN4:PIN4-GFP* (*33*), *pPIN7:PIN7-GFP* (*33*), *DR5rev:GFP* (*35*), *pIAA2:GFP* (*20*), *R2D2* (*36*), *pin1-1;3-5;4-3* (*38*), *pCCS52A1:NLS-GFP* (*29*), *ccs52a1-1* (*29*), *arr2-4* (*29*), and *shy2-31* (*29*) were described previously. *sog1-1* (Col-0/L*er* background) was backcrossed to Col-0 WT three times before use. *atm-2* and *sog1-1* carrying *pARR5:GUS* were generated by crossing the mutants and the *pARR5:GUS* line. Similarly, *pPIN1:PIN1-GFP log7-1* was generated by crossing *pPIN1:PIN1-GFP* and *log7-1*. The full-length open reading frame of *CKX1* was amplified from *Arabidopsis* cDNA by PCR with F_CKX1 (5′-AAAAAGCAGGCTTCATGGGATTGACCTCATCCTTAC-3′) and R_CKX1 (5′-AGAAAGCTGGGTCTTATACAGTTCTAGGTTTCGGC-3′) primers and cloned into the pDONR221 entry vector (Thermo Fisher Scientific) by a BP recombination reaction according to the manufacturer's instructions. The *RCH2* promoter was amplified from *Arabidopsis* genomic DNA by PCR with FP_RCH2 (5′-ATAGAAAAGTTGGGAGGTAAGAATCATGAGAGTGGAG-3′) and RP_RCH2 (5′-TTGTACAAACTTGACATTTGCCTCAAAATACGAAAAGAAG-3′) primers and cloned into the pDONRP4P1R entry vector (Thermo Fisher Scientific) by a BP recombination reaction. To generate the fusion construct of the *RCH2* promoter and *CKX1*, the entry clones were mixed with the R4pGWB601 destination vector (*59*) in an LR recombination reaction according to the manufacturer's instructions (Thermo Fisher Scientific). In addition, the *TIR1* open reading frame was PCR amplified from *Arabidopsis* cDNA with F_TIR1 (5′-AAAAAGCAGGCTTCATGCAGAAGCGAATAGCCTTGTCG-3′) and R_TIR1 (5′-AGAAAGCTGGGTCTTATAATCCGTTAGTAGTAATGATTTGC-3′) primers and cloned

into the pDONR221 entry vector by a BP recombination reaction. To make the *ccvTIR1* entry clones, PCR-mediated site-directed mutagenesis was conducted using the *TIR1* entry vector as a template with F_mTIR1 (5′-GAAAACCTCACGGTGCTGACTTTAATTTGGTACCTGAC-3′) and R_mTIR1 (5′-CAAATTAAAGTCAGCACCGTGAGGTTTTCCTTTAAGCTCCAC-3′) primers. The *WOL* and *TIR1* promoter were PCR amplified from *Arabidopsis* genomic DNA with FP_WOL (5′-ATAGAAAAGTTGGGCAACCCAAATACGAAATACTCGTCC-3′) and RP_WOL (5′-TTGTACAAACTTGAATCTGAGCTACAACAATAGAGAAC-3′) for the *WOL* promoter, and FP_TIR1 (5′-ATAGAAAAGTTGGGGAGTACGAAACCCGAGACTAGGAG-3′) and RP_TIR1 (5′-TTGTACAAACTTGATGCGGCCAAATAACCTCGAGATC-3′) for the *TIR1* promoter, and cloned into the pDONRP4P1R entry vector (Thermo Fisher Scientific) by a BP recombination reaction. To generate the *pWOL:ccvTIR1* and *pTIR1:ccvTIR1* constructs, entry clones were mixed with the R4pGWB601 destination vector (*59*) in an LR recombination reaction. All constructs were introduced into the *Agrobacterium tumefaciens* GV3101 strain harboring the plasmid pMP90. The obtained strains were used to generate stably transformed plants by the floral dip transformation method.

Quantitative RT-PCR

Total RNA was extracted from root tips or whole seedlings with the Plant Total RNA Mini Kit (Favorgen Biotech). First-strand cDNA was prepared from total RNA with ReverTra Ace (Toyobo) according to the manufacturer's instructions. For quantitative PCR, a THUNDERBIRD SYBR qPCR mix (Toyobo) was used with 100 nM primers and first-strand cDNA. PCR reactions were run on a LightCycler 480 real-time PCR system (Roche) according to the following conditions: 95°C for 5 min, 45 cycles at 95°C for 10 s, 60°C for 10 s, and 72°C for 15 s. Transcript levels were normalized to that of *ACTIN2*. Three biological and technical replicates were performed for each experiment. The following primers were used: 5′-CTGGATCGGTGGTTCCATTC-3′ and 5′-CCTGGACCTGCCTCATCATAC-3′ for *ACTIN2*, 5′-AGAGATCACAACGAATCAGATTACGT-3′ and 5′-ATGACGCCGAGGAGATGGT-3′ for *IPT1*, 5′-CGGGTTCGTGTCTGAGAGAG-3′ and 5′-CTGACTTCCTCAACCATTCCA-3′ for *IPT3*, 5′-AGTTACAGCGATGACCACCA-3′ and 5′-GGCAGAGATCTCCGGTAGG-3′ for *IPT5*, 5′-ACTCCTTTGTCTCAAAACGTGTC-3′ and 5′-TGAACACTTCTCTTACTTCTTCGAGT-3′ for *IPT7*, 5′-CATGTTCTAGGGGTCATTCCA-3′ and 5′-CTCCGATGGTCTCACCAGTT-3′ for *CYP735A2*, 5′-GAACTCGGAACCGAACTGG-3′ and 5′-TCAAACCCATTAAACCAATGC-3′ for *LOG1*, 5′-TGATGCTTTTATTGCCTTACCA-3′ and 5′-CCACCGGCTTGTCATGTAT-3′ for *LOG3*, 5′-GTTTGATGGGTTTGGTTTCG-3′ and 5′-CACCGGTCAACTCTCTAGGC-3′ for *LOG4*, 5′-GAGGGTTTGTGTGTTCTGTGGTAGC-3′ and 5′-GAGACCAAACCCATGAGACCAATG-3′ for *LOG5*, 5′-CTCCGATGGTCTCACCAGTT-3′and5′-CATGTTCTAGGGGTCATTCCA-3′ for *LOG7*, 5′-ATTGCACTCCCTGGAGGTTA-3′ and 5′-CCCATCAACATTCAATAGACCA-3′ for *LOG8*, 5′-CTCTCCACGTACTGGTTGTCGTTAC-3′and5′-CGGAAGAGATCTTCACATGTTTGTG-3′ for *PIN1*, 5′-AAGTCACGTACATGCATGTG-3′ and 5′-AGATGCCAACGATAATGAGTG-3′ for *PIN2*, 5′-CTTGCTGGATGAGCTACAGCTTTGG-3′ and 5′-CAAGTCAAACAGCCATGACGCCAAG-3′ for *PIN3*, 5′-CGAAAGAGTAATGCTAGAGGTGGTG-3′ and 5′-AATATCAGTCGTGTCATCACACTTG-3′ for *PIN4*, 5′-CGAAAGAGTAATGCTAGAGGTGGTG-3′and5′-AATATCAGTCGTGTCATCACACTTG-3′ for *PIN7*, 5′-GAAGAATCTACACCTCCTACCAAAA-3′ and 5′-CACGTAGCTCACACTGTTGTTG-3′ for *IAA2*, and 5′-CACGCTGCAAGAGAACAAGA-3′ and 5′-ACCACTTGAGTCCGCATACC-3′ for *CCS52A1*.

GUS staining

Seedlings were incubated in a GUS staining solution [100 mM sodium phosphate, 5-bromo-4-chloro-3-indolyl β-D-glucuronide (1 mg/ml), 0.5 mM ferricyanide, and 0.5 mM ferrocyanide (pH 7.4)] in the dark at 37°C. The samples were cleared with a transparent solution [chloral hydrate, glycerol, and water (8 g:1 ml:1 ml)] and observed under a light microscope (Olympus).

Microscopic observation and measurement of cell death area

Five-day-old roots were stained with 10 μM PI solution for 1 min at room temperature, and root tips were observed under a confocal laser scanning microscope (Olympus, FluoView FV1000). Cell death area was measured using Fiji image analysis software (http://fiji.sc) by defining the field in which PI infiltrates the cells.

Root growth analysis

Seedlings were grown vertically in square plates, and root tips were marked every 24 hours. Plates were photographed, and root growth was calculated by measuring the distance between successive marks along the root axis with ImageJ software (http://rsb.info.nih.gov/ij/).

Quantification of cytokinin levels in isolated cell populations

Protoplasts were isolated from root tips of 5-day-old *pRCH1:GFP* and *pRCH2:CFP* seedlings, which were treated with or without 8 μM zeocin for 24 hours. GFP- or CFP-positive protoplasts were collected through FACS, and their cytokinin concentration was determined using liquid chromatography–tandem mass spectrometry. Protoplast isolation, cell sorting, and cytokinin purification and quantification were performed as described previously (*60*). Analysis and sorting were performed using a BD FACSAria I and BD FACSDiva software. GFP fluorescence was excited using a 488-nm laser and collected using a fluorescein isothiocyanate filter set (emission filter, 530 ± 30 nm), while CFP fluorescence was excited using a 405-nm laser and collected using an Alexa Fluor 430 filter set (emission filter, 550 ± 30 nm). The collected fluorescent protoplasts were snap-frozen in liquid nitrogen after each sorting experiment. Before cytokinin purification and subsequent quantification, the samples were independently collected from four biological replicates per genotype and treatment (60,000 to 160,000 protoplasts per replicate).

EdU pulse labeling

Five-day-old seedlings were grown on MS medium supplemented with or without 8 μM zeocin, 5 nM IAA, or 10 nM cvxIAA for 12 hours and transferred to MS medium with or without zeocin, IAA, or cvxIAA and with 20 μM EdU for 15 min. After washing with MS medium, the seedlings were transferred back to MS medium supplemented with or without zeocin, IAA, or cvxIAA. EdU staining was performed with a Click-iT Plus EdU Alexa Fluor 488 imaging kit (Thermo Fisher Scientific) according to the manufacturer's instructions. Roots were double-stained with EdU and 4′,6-diamidino-2-phenylindole, and epidermis cells were observed with a confocal microscope (FV1000, Olympus).

Statistical analysis

Significant differences between different treatments and genotypes were analyzed by Student's *t* test. Details of statistical analyses are provided in the figure legends.

SUPPLEMENTARY MATERIALS

Supplementary material for this article is available at http://advances.sciencemag.org/cgi/content/full/7/25/eabg0993/DC1

View/request a protocol for this paper from *Bio-protocol*.

REFERENCES AND NOTES

1. M. A. Rounds, P. B. Larsen, Aluminum-dependent root-growth inhibition in *Arabidopsis* results from AtATR-regulated cell-cycle arrest. *Curr. Biol.* **18**, 1495–1500 (2008).
2. T. Sakamoto, Y. T. Inui, S. Uraguchi, T. Yoshizumi, S. Matsunaga, M. Mastui, M. Umeda, K. Fukui, T. Fujiwara, Condensin II alleviates DNA damage and is essential for tolerance of boron overload stress in *Arabidopsis*. *Plant Cell* **23**, 3533–3546 (2011).
3. J. Song, A. F. Bent, Microbial pathogens trigger host DNA double-strand breaks whose abundance is reduced by plant defense responses. *PLOS Pathog.* **10**, e1004030 (2014).
4. V. Garcia, H. Bruchet, D. Camescasse, F. Granier, D. Bouchez, A. Tissier, *AtATM* is essential for meiosis and the somatic response to DNA damage in plants. *Plant Cell* **15**, 119–132 (2003).
5. K. Culligan, A. Tissier, A. Britt, ATR regulates a G2-phase cell-cycle checkpoint in *Arabidopsis thaliana*. *Plant Cell* **16**, 1091–1104 (2004).
6. A. Sancar, L. A. Lindsey-Boltz, K. Ünsal-Kaçmaz, S. Linn, Molecular mechanisms of mammalian DNA repair and the DNA damage checkpoints. *Annu. Rev. Biochem.* **73**, 39–85 (2004).
7. K. Yoshiyama, P. A. Conklin, N. D. Huefner, A. B. Britt, Suppressor of gamma response 1 (*SOG1*) encodes a putative transcription factor governing multiple responses to DNA damage. *Proc. Natl. Acad. Sci. U.S.A.* **106**, 12843–12848 (2009).
8. K. O. Yoshiyama, J. Kobayashi, N. Ogita, M. Ueda, S. Kimura, H. Maki, M. Umeda, ATM-mediated phosphorylation of SOG1 is essential for the DNA damage response in *Arabidopsis*. *EMBO Rep.* **14**, 817–822 (2013).
9. C. A. Sjogren, S. C. Bolaris, P. B. Larsen, Aluminum-dependent terminal differentiation of the *Arabidopsis* root tip is mediated through an ATR-, ALT2-, and SOG1-regulated transcriptional response. *Plant Cell* **27**, 2501–2515 (2015).
10. N. Ogita, Y. Okushima, M. Tokizawa, Y. Y. Yamamoto, M. Tanaka, M. Seki, Y. Makita, M. Matsui, K. Okamoto-Yoshiyama, T. Sakamoto, T. Kurata, K. Hiruma, Y. Saijo, N. Takahashi, M. Umeda, Identifying the target genes of SUPPRESSOR OF GAMMA RESPONSE 1, a master transcription factor controlling DNA damage response in *Arabidopsis*. *Plant J.* **94**, 439–453 (2018).
11. H. Takatsuka, T. Higaki, M. Umeda, Actin reorganization triggers rapid cell elongation in roots. *Plant Physiol.* **178**, 1130–1141 (2018).
12. P. Chen, H. Takatsuka, N. Takahashi, R. Kurata, Y. Fukao, K. Kobayashi, M. Ito, M. Umeda, *Arabidopsis* R1R2R3-Myb proteins are essential for inhibiting cell division in response to DNA damage. *Nat. Commun.* **8**, 635 (2017).
13. S. Adachi, K. Minamisawa, Y. Okushima, S. Inagaki, K. Yoshiyama, Y. Kondou, E. Kaminuma, M. Kawashima, T. Toyoda, M. Matsui, D. Kurihara, S. Matsunaga, M. Umeda, Programmed induction of endoreduplication by DNA double-strand breaks in *Arabidopsis*. *Proc. Natl. Acad. Sci. U.S.A.* **108**, 10004–10009 (2011).
14. N. Fulcher, R. Sablowski, Hypersensitivity to DNA damage in plant stem cell niches. *Proc. Natl. Acad. Sci. U.S.A.* **106**, 20984–20988 (2009).
15. N. Takahashi, N. Ogita, T. Takahashi, S. Taniguchi, M. Tanaka, M. Seki, M. Umeda, A regulatory module controlling stress-induced cell cycle arrest in *Arabidopsis*. *eLife* **8**, e43944 (2019).
16. I. Hwang, J. Sheen, B. Müller, Cytokinin signaling networks. *Annu. Rev. Plant Biol.* **63**, 353–380 (2012).
17. K. Miyawaki, P. Tarkowski, M. Matsumoto-Kitano, T. Kato, S. Sato, D. Tarkowska, S. Tabata, G. Sandberg, T. Kakimoto, Roles of *Arabidopsis* ATP/ADP isopentenyltransferases and tRNA isopentenyltransferases in cytokinin biosynthesis. *Proc. Natl. Acad. Sci. U.S.A.* **103**, 16598–16603 (2006).
18. T. Kiba, K. Takei, M. Kojima, H. Sakakibara, Side-chain modification of cytokinins controls shoot growth in *Arabidopsis*. *Dev. Cell* **27**, 452–461 (2013).
19. T. Kuroha, H. Tokunaga, M. Kojima, N. Ueda, T. Ishida, S. Nagawa, H. Fukuda, K. Sugimoto, H. Sakakibara, Functional analyses of LONELY GUY cytokinin-activating enzymes reveal the importance of the direct activation pathway in *Arabidopsis*. *Plant Cell* **21**, 3152–3169 (2009).
20. A. Bishopp, S. Lehesranta, A. Vatén, H. Help, S. El-Showk, B. Scheres, K. Helariutta, A. P. Mähönen, H. Sakakibara, Y. Helariutta, Phloem-transported cytokinin regulates polar auxin transport and maintains vascular pattern in the root meristem. *Curr. Biol.* **21**, 927–932 (2011).
21. D. Ko, J. Kang, T. Kiba, J. Park, M. Kojima, J. Do, K. Y. Kim, M. Kwon, A. Endler, W. Y. Song, E. Martinoia, H. Sakakibara, Y. Lee, *Arabidopsis* ABCG14 is essential for the root-to-shoot translocation of cytokinin. *Proc. Natl. Acad. Sci. U.S.A.* **111**, 7150–7155 (2014).
22. L. Laplaze, E. Benkova, I. Casimiro, L. Maes, S. Vanneste, R. Swarup, D. Weijers, V. Calvo, B. Parizot, M. B. Herrera-Rodriguez, R. Offringa, N. Graham, P. Doumas, J. Friml, D. Bogusz, T. Beeckman, M. Bennett, Cytokinins act directly on lateral root founder cells to inhibit root initiation. *Plant Cell* **19**, 3889–3900 (2007).
23. R. Dello Ioio, K. Nakamura, L. Moubayidin, S. Perilli, M. Taniguchi, M. T. Morita, T. Aoyama, P. Costantino, S. Sabatini, A genetic framework for the control of cell division and differentiation in the root meristem. *Science* **322**, 1380–1384 (2008).
24. L. O. M. Davis, N. Ogita, S. Inagaki, N. Takahashi, M. Umeda, DNA damage inhibits lateral root formation by up-regulating cytokinin biosynthesis genes in *Arabidopsis thaliana*. *Genes Cells* **21**, 1195–1208 (2016).
25. I. B. D'Agostino, J. Deruère, J. J. Kieber, Characterization of the response of the *Arabidopsis* response regulator gene family to cytokinin. *Plant Physiol.* **124**, 1706–1717 (2000).
26. J. Berdy, Bleomycin-type antibiotics, in *Amino Acid and Peptide Antibiotics*, J. Berdy, Ed. (CRC Press, 1980), pp 459–497.
27. E. Zürcher, D. Tavor-Deslex, D. Lituiev, K. Enkerli, P. T. Tarr, B. Müller, A robust and sensitive synthetic sensor to monitor the transcriptional output of the cytokinin signaling network *in planta*. *Plant Physiol.* **161**, 1066–1075 (2013).
28. R. Dello Ioio, F. S. Linhares, E. Scacchi, E. Casamitjana-Martinez, R. Heidstra, P. Costantino, S. Sabatini, Cytokinins determine *Arabidopsis* root-meristem size by controlling cell differentiation. *Curr. Biol.* **17**, 678–682 (2007).
29. N. Takahashi, T. Kajihara, C. Okamura, Y. Kim, Y. Katagiri, Y. Okushima, S. Matsunaga, I. Hwang, M. Umeda, Cytokinins control endocycle onset by promoting the expression of an APC/C activator in *Arabidopsis* roots. *Curr. Biol.* **23**, 1812–1817 (2013).
30. T. Werner, V. Motyka, V. Laucou, R. Smets, H. Van Onckelen, T. Schmülling, Cytokinin-deficient transgenic *Arabidopsis* plants show multiple developmental alterations indicating opposite functions of cytokinins in the regulation of shoot and root meristem activity. *Plant Cell* **15**, 2532–2550 (2003).
31. S. Gajdosová, L. Spíchal, M. Kamínek, K. Hoyerová, O. Novák, P. I. Dobrev, P. Galuszka, P. Klíma, A. Gaudinová, E. Zizková, J. Hanus, M. Dancák, B. Trávnícek, B. Pesek, M. Krupicka, R. Vanková, M. Strnad, V. Motyka, Distribution, biological activities, metabolism, and the conceivable function of *cis*-zeatin-type cytokinins in plants. *J. Exp. Bot.* **62**, 2827–2840 (2011).
32. K. Miyawaki, M. Matsumoto-Kitano, T. Kakimoto, Expression of cytokinin biosynthetic isopentenyltransferase genes in *Arabidopsis*: Tissue specificity and regulation by auxin, cytokinin, and nitrate. *Plant J.* **37**, 128–138 (2004).
33. E. Feraru, J. Friml, PIN polar targeting. *Plant Physiol.* **147**, 1553–1559 (2008).
34. A. Vieten, S. Vanneste, J. Wisniewska, E. Benková, R. Benjamins, T. Beeckman, C. Luschnig, J. Friml, Functional redundancy of PIN proteins is accompanied by auxin-dependent cross-regulation of PIN expression. *Development* **132**, 4521–4531 (2005).
35. E. Benková, M. Michniewicz, M. Sauer, T. Teichmann, D. Seifertová, G. Jürgens, J. Friml, Local, efflux-dependent auxin gradients as a common module for plant organ formation. *Cell* **115**, 591–602 (2003).
36. C. Y. Liao, W. Smet, G. Brunoud, S. Yoshida, T. Vernoux, D. Weijers, Reporters for sensitive and quantitative measurement of auxin response. *Nat. Methods* **12**, 207–210 (2015).
37. N. Geldner, J. Friml, Y. D. Stierhof, G. Jürgens, K. Palme, Auxin transport inhibitors block PIN1 cycling and vesicle trafficking. *Nature* **413**, 425–428 (2001).
38. J. Friml, A. Vieten, M. Sauer, D. Weijers, H. Schwarz, T. Hamann, R. Offringa, G. Jürgens, Efflux-dependent auxin gradients establish the apical-basal axis of *Arabidopsis*. *Nature* **426**, 147–153 (2003).
39. N. Uchida, K. Takahashi, R. Iwasaki, R. Yamada, M. Yoshimura, T. A. Endo, S. Kimura, H. Zhang, M. Nomoto, Y. Tada, T. Kinoshita, K. Itami, S. Hagihara, K. U. Torii, Chemical hijacking of auxin signaling with an engineered auxin-TIR1 pair. *Nat. Chem. Biol.* **14**, 299–305 (2018).
40. J. J. Petricka, M. A. Schauer, M. Megraw, N. W. Breakfield, J. W. Thompson, S. Georgiev, E. J. Soderblom, U. Ohler, M. A. Moseley, U. Grossniklaus, P. N. Benfey, The protein expression landscape of the *Arabidopsis* root. *Proc. Natl. Acad. Sci. U.S.A.* **109**, 6811–6818 (2012).
41. W. M. Gray, J. C. del Pozo, L. Walker, L. Hobbie, E. Risseeuw, T. Banks, W. L. Crosby, M. Yang, H. Ma, M. Estelle, Identification of an SCF ubiquitin-ligase complex required for auxin response in *Arabidopsis thaliana*. *Genes Dev.* **13**, 1678–1691 (1999).
42. J. F. R. Kerr, A. H. Wyllie, A. R. Currie, Apoptosis: A basic biological phenomenon with wide-ranging implications in tissue kinetics. *Br. J. Cancer* **26**, 239–257 (1972).
43. R. K. Yadav, T. Girke, S. Pasala, M. Xie, G. V. Reddy, Gene expression map of the *Arabidopsis* shoot apical meristem stem cell niche. *Proc. Natl. Acad. Sci. U.S.A.* **106**, 4941–4946 (2009).
44. R. Di Mambro, N. Svolacchia, R. Dello Ioio, E. Pierdonati, E. Salvi, E. Pedrazzini, A. Vitale, S. Perilli, R. Sozzani, P. N. Benfey, W. Busch, P. Costantino, S. Sabatini, The lateral root cap acts as an auxin sink that controls meristem size. *Curr. Biol.* **29**, 1199–1205.e4 (2019).

45. A. S. Hemerly, P. Ferreira, J. de Almeida Engler, M. Van Montagu, G. Engler, D. Inzé, *cdc2a* expression in *Arabidopsis* is linked with competence for cell division. *Plant Cell* **5**, 1711–1723 (1993).
46. K. Himanen, E. Boucheron, S. Vanneste, J. de Almeida Engler, D. Inzé, T. Beeckman, Auxin-mediated cell cycle activation during early lateral root initiation. *Plant Cell* **14**, 2339–2351 (2002).
47. T. Ishida, S. Adachi, M. Yoshimura, K. Shimizu, M. Umeda, K. Sugimoto, Auxin modulates the transition from the mitotic cycle to the endocycle in *Arabidopsis*. *Development* **137**, 63–71 (2010).
48. Z. Magyar, L. De Veylder, A. Atanassova, L. Bakó, D. Inzé, L. Bögre, The role of the *Arabidopsis* E_2FB transcription factor in regulating auxin-dependent cell division. *Plant Cell* **17**, 2527–2541 (2005).
49. V. Boudolf, K. Vlieghe, G. T. Beemster, Z. Magyar, J. A. Torres Acosta, S. Maes, E. Van Der Schueren, D. Inzé, L. De Veylder, The plant-specific cyclin-dependent kinase CDKB1;1 and transcription factor E2Fa-DPa control the balance of mitotically dividing and endoreduplicating cells in *Arabidopsis*. *Plant Cell* **16**, 2683–2692 (2004).
50. B. Canher, J. Heyman, M. Savina, A. Devendran, T. Eekhout, I. Vercauteren, E. Prinsen, R. Matosevich, J. Xu, V. Mironova, L. De Veylder, Rocks in the auxin stream: Wound-induced auxin accumulation and *ERF115* expression synergistically drive stem cell regeneration. *Proc. Natl. Acad. Sci. U.S.A.* **117**, 16667–16677 (2020).
51. J. Hasegawa, T. Sakamoto, S. Fujimoto, T. Yamashita, T. Suzuki, S. Matsunaga, Auxin decreases chromatin accessibility through the TIR1/AFBs auxin signaling pathway in proliferative cells. *Sci. Rep.* **8**, 7773 (2018).
52. M. Endo, Y. Ishikawa, K. Osakabe, S. Nakayama, H. Kaya, T. Araki, K. Shibahara, K. Abe, H. Ichikawa, L. Valentine, B. Hohn, S. Toki, Increased frequency of homologous recombination and T-DNA integration in *Arabidopsis* CAF-1 mutants. *EMBO J.* **25**, 5579–5590 (2006).
53. F. Lozano-Elena, A. Planas-Riverola, J. Vilarrasa-Blasi, R. Schwab, A. I. Caño-Delgado, Paracrine brassinosteroid signaling at the stem cell niche controls cellular regeneration. *J. Cell Sci.* **131**, jcs204065 (2018).
54. A. P. Mähönen, A. Bishopp, M. Higuchi, K. M. Nieminen, K. Kinoshita, K. Törmäkangas, Y. Ikeda, A. Oka, T. Kakimoto, Y. Helariutta, Cytokinin signaling and its inhibitor AHP6 regulate cell fate during vascular development. *Science* **311**, 94–98 (2006).
55. M. Bonke, S. Thitamadee, A. P. Mähönen, M. T. Hauser, Y. Helariutta, APL regulates vascular tissue identity in *Arabidopsis*. *Nature* **426**, 181–186 (2003).
56. R. Heidstra, D. Welch, B. Scheres, Mosaic analyses using marked activation and deletion clones dissect *Arabidopsis* SCARECROW action in asymmetric cell division. *Genes Dev.* **18**, 1964–1969 (2004).
57. T. Waki, T. Hiki, R. Watanabe, T. Hashimoto, K. Nakajima, The *Arabidopsis* RWP-RK protein RKD4 triggers gene expression and pattern formation in early embryogenesis. *Curr. Biol.* **21**, 1277–1281 (2011).
58. D. Weijers, E. Benkova, K. E. Jäger, A. Schlereth, T. Hamann, M. Kientz, J. C. Wilmoth, J. W. Reed, G. Jürgens, Developmental specificity of auxin response by pairs of ARF and Aux/IAA transcriptional regulators. *EMBO J.* **24**, 1874–1885 (2005).
59. S. Nakamura, S. Mano, Y. Tanaka, M. Ohnishi, C. Nakamori, M. Araki, T. Niwa, M. Nishimura, H. Kaminaka, T. Nakagawa, Y. Sato, S. Ishiguro, Gateway binary vectors with the bialaphos resistance gene, *bar*, as a selection marker for plant transformation. *Biosci. Biotechnol. Biochem.* **74**, 1315–1319 (2010).
60. I. Antoniadi, L. Plačková, B. Simonovik, K. Doležal, C. Turnbull, K. Ljung, O. Novák, Cell-type-specific cytokinin distribution within the *Arabidopsis* primary root apex. *Plant Cell* **27**, 1955–1967 (2015).

Acknowledgments: We thank T. Kakimoto, A. Britt, Y. Matsubayashi, M. Aida, I. Hwang, T. Nakagawa, S. Miyashima, K. Nakajima, M. T. Morita, J. Friml, and the *Arabidopsis* Biological Research Center for providing *Arabidopsis* mutants, binary vectors, and transgenic plants. We also thank M. Kojima for help in cytokinin measurements. **Funding:** This work was supported by MEXT KAKENHI (grant numbers 22119009, 26113515, 17H06470, and 17H06477) and JSPS KAKENHI (grant numbers 26291061, 26650099, 26840096, and 19K06708). K.L. and I.A. were supported by the Knut and Alice Wallenberg Foundation, the Swedish Research Council, and the Swedish Governmental Agency for Innovation Systems. **Author contributions:** N.T., S.I., K.N., I.A., M.K., and K.L. performed experiments. N.T., S.I., K.N., I.A., M.K., and K.L. performed data analysis. N.T., S.I., H.S., I.A., K.L., and M.U. designed experiments. N.T., K.L., and M.U. wrote the manuscript. **Competing interests:** The authors declare that they have no competing interests. **Data and materials availability:** All data needed to evaluate the conclusions in the paper are present in the paper and/or the Supplementary Materials. Additional data related to this paper may be requested from the authors.

Submitted 10 December 2020
Accepted 28 April 2021
Published 16 June 2021
10.1126/sciadv.abg0993

Citation: N. Takahashi, S. Inagaki, K. Nishimura, H. Sakakibara, I. Antoniadi, M. Karady, K. Ljung, M. Umeda, Alterations in hormonal signals spatially coordinate distinct responses to DNA double-strand breaks in *Arabidopsis* roots. *Sci. Adv.* **7**, eabg0993 (2021).